ANL/NE-16/19

Argonne NATIONAL LABORATORY

The SAS4A/SASSYS-1 Safety Analysis Code System

Nuclear Engineering Division

About Argonne National Laboratory

Argonne is a U.S. Department of Energy laboratory managed by UChicago Argonne, LLC under contract DE-AC02-06CH11357. The Laboratory's main facility is outside Chicago, at 9700 South Cass Avenue, Argonne, Illinois 60439. For information about Argonne and its pioneering science and technology programs, see www.anl.gov.

Document Availability

Online Access: U.S. Department of Energy (DOE) reports produced after 1991 and a growing number of pre-1991 documents are available free via DOE's SciTech Connect (http://www.osti.gov/scitech/)

Reports not in digital format may be purchased by the public from the National Technical Information Service (NTIS):

U.S. Department of Commerce
National Technical Information Service
5301 Shawnee Rd
Alexandria, VA 22312
www.ntis.gov
Phone: (800) 553-NTIS (6847) or (703) 605-6000
Fax: (703) 605-6900
Email: **orders@ntis.gov**

Reports not in digital format are available to DOE and DOE contractors from the Office of Scientific and Technical Information (OSTI):

U.S. Department of Energy
Office of Scientific and Technical Information
P.O. Box 62
Oak Ridge, TN 37831-0062
www.osti.gov
Phone: (865) 576-8401
Fax: (865) 576-5728
Email: **reports@osti.gov**

Disclaimer

ANL/NE-16/19

The SAS4A/SASSYS-1 Safety Analysis Code System

Chapter 11:
FPIN2: Pre-Failure Metal Fuel Pin Behavior Model

T. Sofu and J. M. Kramer
Nuclear Engineering Division
Argonne National Laboratory

March 31, 2017

TABLE OF CONTENTS

LIST OF FIGURES

LIST OF TABLES

NOMENCLATURE

Subscript	Description
l	Fully annealed material
θ	Angular direction in cylindrical coordinates
0,o	Initial, reference
c	Cladding
ci	Cladding inner radius
e	Equivalent
f	Fuel
f	Failure
fo	Fuel out radius
g	Gas
gb	Grain boundary
i	Time step index
i	Radial element index
I, II	Element types
j	Axial segment index
m	Mean, average
n	Iteration index
N	Iteration index
Na	Sodium
pu	True plastic (strain)
r	Radial direction in cylindrical coordinates
r	Rupture
s	Saturation
th	Threshold
u	True/ultimate (stress)
z	Axial direction in cylindrical coordinates

Superscript	Description
Θ	Thermal (strain)
a	Apparent (strain)
c	Crack (strain)
C	Cavity

e	Elastic (strain)
ext	External loads
G	Fuel-cladding gap
i	Iteration counter
int	Internal stress field
IGL	Ideal gas law
MECH	Mechanical analysis
p	Plastic (strain)
ps	Pseudo (stress)
P	Plenum
ref	Reference
s	Swelling (strain)
t	Total (strain)
T	Total

Notation	**Description**
¯(overline)	Equivalent
_(underline)	Indicates a vector
·(dot)	Indicates derivative with respect to time
ˆ(hat)	Indicates a unit vector
[]	Indicates a matrix
{}^{T}	Transpose of a vector
∇	Gradient

Symbol	**Description**
α	Thermal expansion coefficient
δ	Nodal displacement
$\Delta L/L_0$	Linear thermal expansion
Δt	Time step size
ε	Strain
$\hat{\varepsilon}$	Cladding hardness parameter
ϕ	Overpressure in grain boundary bubble growth model
ϕ	Finite element displacement function
γ	Specific surface free energy in surface tension restraint term
ν	Poisson's ratio

Ω	Atomic volume in grain boundary bubble growth model
ψ	Constant in finite element displacement function in axial direction
ρ	Radius of curvature in surface tension restraint term
ρ	Density
σ	Stress
θ	Intersection angle between the bubble surface and grain boundary
θ	Initial hardening rate
a	Finite element inner radius
A	Area of intersection between the finite elements
b	Finite element outer radius
B	Matrix in equilibrium equation
C	Curve bounding A
C	Matrix in generalized Hooke's law
C	Material functions in secondary creep equation
$d\varepsilon$	Incremental strain
$d\lambda$	Proportionality factor for plastic strain increments
$d\sigma$	Incremental stress
dp	Pressure increment
D	Grain size
D	Diffusion coefficient in grain boundary bubble growth model
E	Young's modulus
F	Constitutive function for plastic strains
F	Force
F	Axial force
$\dot{F}$	Fission rate
G	Constitutive function for swelling strains
G	Shear modulus
$\hat{i}$	Unit vector in coordinate directions
K	Stiffness matrix
K	Bulk modulus
L	Finite element radial thickness
M	Rate sensitivity parameter in cladding yield and saturation flow stresses
M	Mass
$\dot{M}$	Eutectic penetration rate

$\hat{n}$	Outward normal to the finite element surface, S
N	Finite element shape function
N	Number density of gas bubbles in grain boundary bubble growth model
P	Pressure
Q	Activation energy in secondary creep equation
Q	Thermal modulus
R	Residual in iterative solution of equilibrium equations
R	Radius
R	Gas constant
S	Deviatoric stress
S	Surface area of finite element
T	Time
T	Elements of load vector in equilibrium equation expressing external forces
T	Temperature
U	Displacement in radial coordinate direction
V	Displacement in θ coordinate direction
V	Volume of finite element
W	Grain boundary thickness
W	Displacement in axial coordinate direction
W	Gradient vector for plastic strain increments
Z	Zener-Holloman parameter

FPIN2: PRE-FAILURE METAL FUEL PIN BEHAVIOR MODEL

11.1 Introduction

Since fuel element behavior during fast reactor transients can significantly affect accident energetics, an accurate and detailed model for the mechanical response of fuel elements is needed in safety assessments. During transients that lead to overheating of fuel and cladding, plastic straining of the cladding due to internal fission gas pressure and differential expansion between the fuel and cladding may result in cladding rupture and release of fission products to the primary coolant. In addition to the fundamental concern for cladding failure, fuel axial expansion can also have an important role due to the associated negative reactivity potential.

FPIN2 is a validated computer code that provides mathematical models that simulate fuel and cladding mechanical response and predict fuel element performance over a wide range of transients. It performs an analysis of metal fuel and cladding deformation, including the impact of fuel-cladding interactions, and estimates cladding failure locations and times.

FPIN2 has been incorporated into the SASSYS/SAS4A code system for mechanical analysis of individual fuel elements. In this implementation, SASSYS/SAS4A provides fuel and cladding temperatures, and FPIN2 performs the analysis of fuel element deformation and predicts the time and location of cladding failure. FPIN2 results are also used for the estimates of axial fuel expansion and the associated reactivity effects. In this chapter, FPIN2's mechanical model, the SAS-FPIN2 coupling methodology, and the integrated SAS-FPIN2 model usage are presented.

11.1.1 Brief Description of FPIN2

The FPIN2 code has been developed to analyze the thermal-mechanical phenomena that control fuel element behavior during fast reactor transients. The early versions of the code were based on the characteristics of oxide and carbide ceramic fuels [11-1,11-2]. More recently, FPIN2 has been adapted for the analysis of metallic fuels [11-3,11-4]. The overall modeling for this metallic fuel version of the code was validated through comparison of FPIN2 calculations with the data from TREAT tests on EBR-II irradiated fuel, prototypic of the IFR concept [11-5,11-6]. The most recent version of the code integrated with SASSYS/SAS4A includes numerous model improvements that reflect the experience gained during these validation efforts.

A wide range of material behavior is modeled in the code that describes elastic, plastic, thermal, and swelling performance of fuel elements. Since the primary emphasis in FPIN2 is on the mechanical analysis of the fuel and cladding, in the standalone version of the code temperatures are calculated using a simple model based on pin-in-a-pipe geometry and single-phase flow. The mechanical model, on the other hand, is based on a rigorous force-displacement formulation and uses an implicit finite element method with linear shape functions. The finite element scheme used allows convenient modular coding in which different models for material behavior and improvements in specific algorithms are easily implemented. The equilibrium equations are derived form equations of virtual work. The elements are defined in an

(r,z) mesh; however, axial symmetry and generalized plane strain are assumed so that the analysis is essentially one-dimensional. The elements are allowed to interact only at the radial boundaries (nodes), and the displacements within the elements are approximated by linear functions of the nodal displacements.

Additional models for metallic fuels such as models for fission gas generation and release, molten cavity formation, the large gas plenum, and fuel-cladding eutectic alloy formation are also provided in FPIN2 to complement the fuel element mechanics calculations. Internal pin pressure is determined from direct mass and volume balances in the central cavity and gas plenum. The molten fuel cavity in FPIN2 is located by the axial and radial extent to which the fuel has reached its solidus temperature and the elements inside the cavity boundary are dropped out of the stress-chain calculation. For cases where initial fuel melting occurs below the top axial segment, the plenum pressure calculation is decoupled from the molten cavity pressure calculation. Once melting reaches cavity-gas plenum interface, the two pressures are assumed to equilibrate and the plenum/cavity pressure-volume equations are solved together to give a common pin pressure and amount of molten fuel extruded into the plenum.

Checking rupture is predicted in the code by using the life fraction criterion. The life fraction change over a time step is determined from the change in rupture time for the instantaneous average cladding temperature and the hoop stress obtained form the thin-shell equations used in developing the life fraction correlations. The effect of low melting point eutectic formation between the fuel and the cladding is included in the calculations by considering only the thickness of unaffected cladding that is available to carry the load.

11.1.2 Overview

The finite element formulation that constitutes the basic structure of FPIN2's mechanics calculation is described in Section 11.2. Although the models presented in Section 11.2 are primarily developed for oxide fuel, they provide a substantially robust structure that allows modifications to handle metallic fuels. The modifications and additions to the code for metal fuels are discussed separately in Section 11.3. Most of these models for metallic fuels reflect the experience gained during FPIN2 validation efforts through comparison with the data from TREAT tests.

Two modes of SAS-FPIN2 coupled operations are provided. In the stand-alone mode, independent FPIN2 input is used and FPIN2 is executed without interfacing to SASSYS/SAS4A. In the interfaced mode, SASSYS/SAS4A calculated fuel and cladding temperatures are transferred to FPIN2, and FPIN2 results are used in the analysis of fuel behavior. The SAS-FPIN2 coupling methodology and the integrated SAS-FPIN2 model usage along with input and output descriptions are presented in Section 11.4.

11.2 Fuel Element Mechanics

The mechanical model of FPIN2 uses an implicit finite element method based on a force-displacement formulation. The elements are defined by dividing the fuel and cladding into a number of axial segments and radial rings. Axial symmetry of the loads

and generalized plane strain are assumed; therefore, the elements are allowed to interact only at the radial boundaries (nodes). The displacements within the elements are approximated by linear functions.

The mechanical analysis of FPIN2 basically provides the fuel and cladding stresses, σ, and nodal displacements, δ, for each element during overpower and undercooling events. The fuel and cladding behavior model includes thermal expansions, elastic/plastic/creep deformations, cracking, and melting. A continuous cracking model is used in which an element is assumed to crack in the radial direction when the tensile stress exceeds the fracture stress. Pre-existing cracks are also handled by specifying initial crack strains.

The finite element equilibrium equations are derived from equations of virtual work that leads to a force balance between the external and internal forces

$$\underline{f}^{\text{int}}(\sigma) = \underline{f}^{ext} \tag{11.2-1}$$

The external source vector in this equation, $\underline{f}^{ext}$, describes the external loads at the cavity boundary and the cladding outer surfaces, and the internal force vector, $\underline{f}^{\text{int}}(\sigma)$, depends on the unknown stress field that must be found to satisfy Eq. 11.2-1 and the constitutive laws for the materials. When this generally non-linear set is linearized and the equations for both the fuel and cladding elements are assembled together for the unknown nodal displacements at each axial segment, the resulting linear equation set can be written symbolically as

$$[K]\,\underline{\delta} = \underline{f} \tag{11.2-2}$$

where [*K*] is the stiffness matrix. An elastic-plastic approximation is used in FPIN2 to derive the elements of the stiffness matrix involving the total derivatives of the constitutive equations. The force vector in Eq. 11.2-2 includes the external loads, thermal and other initial strains, and pseudo-forces involving approximations to the plastic and/or creep strains.

The equilibrium equations (Eq. 11.2-1) and the linear equations (Eq. 11.2-2) are solved iteratively for each axial segment by making use of residuals. In this scheme, first the stiffness matrix, [*K*], and an initial guess for the force vector, $\underline{f}_0$, are assembled using available information from the previous time step. Then, the linear equations (Eq. 11.2-2) are solved for the new nodal displacements, and from them the increments of total strain are obtained. Assuming that the total material strain is a superposition of elastic, plastic, thermal, and swelling strains, the elastic component of the increments of total strain is separated (see Section 11.2.2) and used to calculate the stress field throughout the fuel element that satisfies the material constitutive equations. These stresses, then, are used to obtain the residuals form the equilibrium equations (Eq. 11.2-1) as follows

$$\underline{r}_n = \underline{f}^{ext} - \underline{f}^{\text{int}}(\sigma_n) \tag{11.2-3}$$

where *n* is the iteration index. Using these residuals, the initial estimate for the force vector in linear equations (Eq. 11.2-2) is modified according to

$$\underline{f}_{n+1} = \underline{f}_n + \underline{r}_n \tag{11.2-4}$$

The procedure is repeated until convergence is established. This basic scheme is generalized in FPIN2 to include analysis of additional material performance in fuel and cladding such as cracking and melting.

The details of this procedure described above are given in the following sections. The basic stress, strain, and nodal displacement relationships are discussed in Section 11.2.1, and the algorithm for separating elastic strain from the total strain is presented in Section 11.2.2. FPIN2 uses a continuous cracking model that permits cracks in the radial plane. The principles of this model are described in Section 11.2.3. The finite element formulation and the details of the implicit solution scheme outlined above are presented in Section 11.2.4. The formulations given in the aforementioned sections are based on updated geometry and can handle large strains. This is accomplished by performing the mechanics calculation on an incremental basis and updating the fuel element geometry at the end of each time step as described in Section 11.2.5.

11.2.1 Basic Stress-Strain-Displacement Equations

In this section, a number of definitions and basic equations relating stresses, strains, and modal displacements are collected and presented in a uniform notation. These equations constitute the foundation of FPIN2's mechanics model and serve as the basis for derivations in later sections. Formulas are derived for large-strain finite element analysis of deformation in a cylindrical fuel element under accident conditions. At the beginning of the analysis, the fuel element is assumed to be stress-free with steady-state thermal conditions. Thermoeleastic-plastic behavior is assumed for both the fuel and cladding. Swelling (including hot-pressing) and cracking are also allowed in both materials.

Fuel elements are assumed to consist of a number of axial segments. The finite elements are defined in each axial segment separately and allowed to interact only at the radial boundaries (nodes). The displacements within the elements are approximated by linear functions of the nodal displacements. Axial symmetry of temperatures and external loads is assumed; therefore, the finite elements can be viewed as a series of concentric annular rings. The generalized plane strain assumption is used describe the interaction between the axial segments.

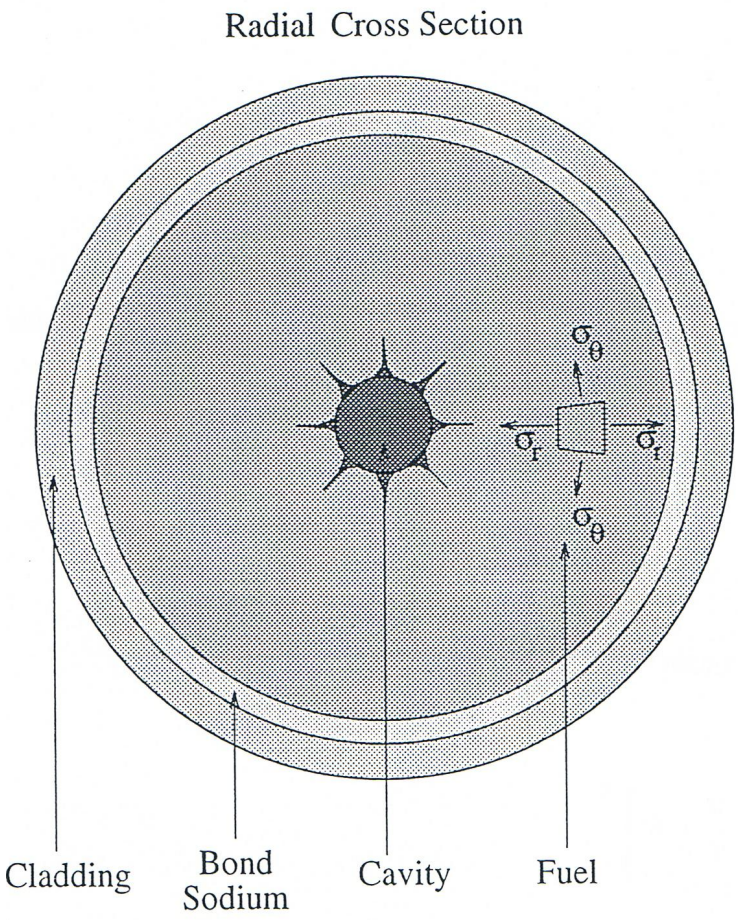

Fig. 11.2-1: FPIN2 Geometry

Each axial segment is allowed to have regions containing central cavity gas and/or molten fuel, regions of solid material that are uncracked, and regions that contain radial cracks (Fig. 11.2-1). If an element does not contain any cracks, the axisymmetry assumption dictates that the deformation depends only on *r*. Although the existence of radial cracks, in general, destroys this symmetry, it is assumed that the number of cracks in an element is large enough to make the deformation essentially axisymmetric.

11.2.1.1 Strain-Displacement Relationships

In cylindrical coordinates, the strain-displacement relations are given by

$$\underline{\varepsilon}^t = \left\{\varepsilon_r^t, \varepsilon_\theta^t, \varepsilon_z^t\right\}^T = \left\{\frac{\partial u}{\partial r}, \frac{u}{r} + \frac{1}{r}\frac{\partial v}{\partial \theta}, \frac{\partial w}{\partial z}\right\}^T \tag{11.2-5}$$

where *u*, *v*, and *w* are displacements in *r*, θ and *z* coordinate directions, respectively. If the material is continuous, the deformation depends only on *r* due to axisymmetry of

temperatures and loads. If the material contains radial cracks, the tangential displacement, v, can be expressed as a linear function of θ in a first order approximation assuming that sufficiently numerous radial cracks exist in the element. In the axial direction, the generalized plane strain condition requires that

$$w = \psi z \tag{11.2-6}$$

where ψ is a constant.

For convenience, we may rewrite the strain-displacement relation as follows to differentiate the crack strain from continuous material strain

$$\underline{\varepsilon}^{t} = \underline{\varepsilon}^{a} + \underline{\varepsilon}^{c} \tag{11.2-7}$$

where "apparent total strain" and "crack strain" vectors are given respectively by

$$\underline{\varepsilon}^{a} = \left\{ \frac{du}{dr}, \frac{u}{r}, \psi \right\}^{T} \tag{11.2-8}$$

$$\underline{\varepsilon}^{c} = \left\{ 0, \varepsilon_{\theta}^{c}, 0 \right\}^{T} \tag{11.2-9}$$

Here, $\underline{\varepsilon}_{\theta}^{c}$ is the unknown crack strain component related to radial creaks in the material.

11.2.1.2 Components of Total Strain

The total material strain, $\underline{\varepsilon}^{t}$, can be written as the sum of the elastic strain, $\underline{\varepsilon}^{e}$, the plastic strain, $\underline{\varepsilon}^{p}$, the thermal strain, $\underline{\varepsilon}^{\theta}$, and the swelling strain, $\underline{\varepsilon}^{s}$:

$$\underline{\varepsilon}^{t} = \underline{\varepsilon}^{e} + \underline{\varepsilon}^{p} + \underline{\varepsilon}^{\theta} + \underline{\varepsilon}^{s} \tag{11.2-10}$$

11.2.1.2.1 Elastic Strain

In linear elasticity, the components of elastic strain are related to normal stresses through the generalized Hook's law

$$\underline{\sigma} = [C]\underline{\varepsilon}^{e} \tag{11.2-11}$$

where the matrix [C] is given in terms of Young's modulus, E, and Poisson's ratio, ν, as follows

$$[C]=\frac{E(1-\nu)}{(1+\nu)(1-2\nu)}\begin{bmatrix} 1 & \frac{\nu}{(1-\nu)} & \frac{\nu}{(1-\nu)} \\ \frac{\nu}{(1-\nu)} & 1 & \frac{\nu}{(1-\nu)} \\ \frac{\nu}{(1-\nu)} & \frac{\nu}{(1-\nu)} & 1 \end{bmatrix} \tag{11.2-12}$$

In general, the elastic parameters E and ν are functions of temperature, T.

11.2.1.2.2 Thermal Strain

In the original oxide fuel version of FPIN2, the components of isotropic thermal strain, $\underline{\varepsilon}^{\theta}$, are expressed in terms of mean thermal expansion coefficient, α_m, as follows

$$\varepsilon_r^{\Theta}=\varepsilon_\theta^{\Theta}=\varepsilon_z^{\Theta}=\alpha_m\left(T-T_0\right) \tag{11.2-13}$$

where T_0 is a reference temperature. In more recent applications for metallic fuels, the thermal expansion is expressed in terms of handbook linear thermal expansion data [11-7], $\Delta L/L_0$, as discussed in Section 11.3.3. Using the thermal data provides more detailed information since it automatically includes the total fuel expansion at solid-to-solid phase transitions. Any other stress-independent isotropic swelling strains (such as selling due to solid fission products or small surface tension dominated gas bubbles) are treated in the same manner as thermal strains in the model.

11.2.1.2.3 Swelling strain

Stress dependent swelling strains, $\underline{\varepsilon}^{s}$, due to fission gas in the fuel are also assumed to be isotropic and required to be expressed by an implicit function of the form

$$g\left(\sigma_m,\varepsilon^s,d\varepsilon^s/dt,T,\nabla T,\rho\right)=0 \tag{11.2-14}$$

Here, the mean hydrostatic stress σ_m is calculated from

$$\sigma_m=\frac{\sigma_r+\sigma_\theta+\sigma_z}{3} \tag{11.2-15}$$

Hot-pressing is also considered in the model as a negative contribution to the total swelling.

11.2.1.2.4 Plastic strain

The plastic deformation of the material is postulated to occur when a generalized *von Mises* flow condition is satisfied:

$$f\left(\sigma_e, \bar{\varepsilon}^p, d\bar{\varepsilon}^p/dt, T\right) = 0 \tag{11.2-16}$$

where the equivalent stress, σ_e, and equivalent plastic strain, $\bar{\varepsilon}^p$, are given respectively by the following equations

$$\sigma_e = \sqrt{\frac{3}{2}\left(S_r^2 + S_\theta^2 + S_z^2\right)} \tag{11.2-17}$$

$$\bar{\varepsilon}^p = \int d\bar{\varepsilon}^p = \int \sqrt{\frac{2}{3}\left[\left(d\varepsilon_r^p\right)^2 + \left(d\varepsilon_\theta^p\right)^2 + \left(d\varepsilon_z^p\right)^2\right]} \tag{11.2-18}$$

with the deviatoric stresses defined as

$$S_i = \sigma_i - \sigma_m \tag{11.2-19}$$

($i = r, \theta, z$). The normality condition of plasticity states that the increment of the plastic strain is proportional to the gradient in stress space of the flow condition:

$$\underline{d\varepsilon}^p = d\lambda\, \underline{W} \tag{11.2-20}$$

where $d\lambda$ is the proportionality factor. The gradient vector is given by

$$\underline{W} = \left\{\frac{\partial\sigma_e}{\partial\sigma_r}, \frac{\partial\sigma_e}{\partial\sigma_\theta}, \frac{\partial\sigma_e}{\partial\sigma_z}\right\}^T = \frac{3}{2\sigma_e}\left\{S_r, S_\theta, S_z\right\}^T \tag{11.2-21}$$

For the particular form of flow conditions chosen in this model, the factor of proportionality, $d\lambda$, is identical to the increment in equivalent plastic strain, $d\bar{\varepsilon}^p$. The plastic strains are assumed to occur with zero volume change:

$$\varepsilon_r^p + \varepsilon_\theta^p + \varepsilon_z^p = 0 \tag{11.2-22}$$

The constitutive equations for plastic deformation as well as swelling (Eqs. 11.2-16 and 11.2-14) indicate that, in general, the deformation depends on the changes in stress and temperature. Also, a major part of the deformation in a fuel element at high temperatures is rate dependent. The discussion of the material properties for the swelling and plastic behavior of the metallic fuel pins is given in Section 11.3.

11.2.1.3 Incremental Stress-Strain Relationships

Since the elastic constants of the matrix [C] in Eq. 11.2-11 are functions of temperature, T, the incremental elastic stress components are given by

$$\underline{d\sigma} = [C]\underline{d\varepsilon^e} + \frac{d[C]}{dT}\underline{\varepsilon}^e\, dT = [C]\left(d\varepsilon^e - \frac{d[C]^{-1}}{dT}\underline{\sigma}\, dT\right) \tag{11.2-23}$$

Using the equation representing the superposition of strains:

$$\underline{d\varepsilon}^e = \underline{d\varepsilon}^t - \underline{d\varepsilon}^p - \underline{d\varepsilon}^\Theta - \underline{d\varepsilon}^s \tag{11.2-24}$$

and replacing $\underline{d\varepsilon}^p$ with equivalent plastic strain increments, the change in stress can be expressed in terms of increment of total strain as follows

$$\underline{d\sigma} = [C]\left(\underline{d\varepsilon}^t - \underline{W}d\bar{\varepsilon}^p - \underline{Q}dT - \underline{d\varepsilon}^s\right) \tag{11.2-25}$$

where, for convenience, the thermal modulus $\underline{Q}$ has been introduced:

$$\underline{Q} = \underline{\alpha} + \frac{d[C]^{-1}}{dT}\underline{\sigma} \tag{11.2-26}$$

The mechanical model of FPIN2 makes use of Eq. 11.2-25 to calculate approximate changes in stress given the estimates of plastic and swelling strain increments.

11.2.1.4 Element Types

The actual form of Eq. 11.2-25 depends on the type of fuel element considered. Originally, four different types of elements are considered in the finite element formulation of FPIN2 that allows analysis of cracks in both radial and transverse planes. However, only two types of elements are available in the metal fuel version because cracks in metallic fuels, if they occur, are predominantly radial. The definitions of the two types are as follows:

Type I: The element lies in continuous fuel or cladding. Both the axial and tangential crack strains are zero; therefore, the total stain in the element is equal to the apparent total strain. The *resultant* of the axial stress is also assumed to be known.[1]

Type II: The element lies in a portion of the fuel where only radial cracks are present and the tangential crack strain is non-zero. The circumferential stress is constant everywhere in the element and equal to the boundary value $\sigma_\theta = -p_g$ (p_g is the pressure of the fission gas present in the crack opening.) As in Type I, the resultant axial force is assumed to be known.

[1] If the fuel-cladding gap is closed, this resultant axial force may include both fuel and cladding.

Table 11.2-1: Source of Calculated Stress and Strain Results for the Element Types

Element Type		Equilibrium and Strain-Displacement Equations	Crack Strain Definition	Stress Boundary Conditions	Algorithm Described in Section 11.2.2
I	Continuous	ε_r^a , ε_θ^a , ε_z^a	$\varepsilon_\theta^c = 0$	---	σ_r , σ_θ , σ_z
II	Radial cracks	ε_r^a , ε_θ^a , ε_z^a	$\varepsilon_\theta^c \neq 0$	$\sigma_\theta = -p_g$	σ_r , σ_z , ε_θ^c

In each case, solving the finite element equilibrium equations gives the radial displacement, $u(r)$, from which apparent strain, $\underline{\varepsilon}^a$, can be calculated. The stress and strain components not obtained from the equilibrium equations, strain-displacement relations, or stress boundary conditions are calculated by an algorithm to separate elastic strain from the total strain as described in Section 11.2.2 (see Table 11.2-1).

11.2.1.5 Relationships for Stress Increments: Pseudo-Stress

Since the actual form of Eq. 11.2-25 depends on the type of fuel element considered, it can be expressed in following generalized form

$$\underline{d\sigma} = [C]\underline{d\varepsilon}^a - \underline{d\sigma}^{ps} \tag{11.2-27}$$

where $\underline{d\sigma}^{ps}$ is the incremental pseudo-stress. Ad described in Section 11.2.4.2, given the estimates of plastic and swelling strain increments, this pseudo-stress term is treated as a constant within a time step. In other words, Eq. 11.2-27 expresses the changes in stress in terms of a known term $\underline{d\sigma}^{ps}$ and an unknown increment $\underline{d\varepsilon}^a$. The calculated stress increments are then corrected to satisfy the equilibrium and constitutive equations to a desired accuracy as described in Section 11.2.4.2.

Existence of radial cracks in the element alters the form of the elastic modulus, $[C]$, and the pseudo-stress vector, $\underline{d\sigma}^{ps}$. As shown in Table 11.2-1, for an uncracked element all three components of the total apparent strain are to be found from the equilibrium equations. Therefore, the incremental stress can be written in the form of Eq. 11.2-27 as

$$\underline{d\sigma} = [C]\underline{d\varepsilon}^a - \underline{d\sigma}_I^{ps} \tag{11.2-28}$$

where $[C_I]$ and the incremental pseudo-stress are simply defined by

$$[C_I] = [C] \tag{11.2-29}$$

and

$$\underline{d\sigma_I^{ps}} = [C]\left(\underline{Q}\,dT + \underline{W}\,d\bar{\varepsilon}^{\,p} + \underline{d\varepsilon^s}\right) \tag{11.2-30}$$

For an element with radial cracks (Type II), Table 11.2-1 indicates that

$$\underline{d\varepsilon^c} = \left\{0, d\varepsilon_\theta^c, 0\right\}^T \tag{11.2-31}$$

$$\underline{d\sigma} = \left\{d\sigma_r, -dp_g, d\sigma_z\right\}^T \tag{11.2-32}$$

By substituting these equations into Eq. 11.2-25 and premultiplying by $[C]^{-1}$, $d\varepsilon_\theta^c$ can be eliminated and the equations can be solved for $d\sigma_r$ and $d\sigma_z$. The result can be written in the form of Eq. 11.2-28 as

$$\underline{d\sigma} = [C_{II}]\underline{d\varepsilon^a} - \underline{d\sigma_{II}^{ps}} \tag{11.2-33}$$

where for Type II elements

$$[C_{II}] = \frac{E}{1-\nu^2}\begin{bmatrix} 1 & 0 & \nu \\ 0 & 0 & 0 \\ \nu & 0 & 1 \end{bmatrix} \tag{11.2-34}$$

and

$$\underline{d\sigma_{II}^{ps}} = \frac{E}{1-\nu^2}\begin{bmatrix} 1 & 0 & \nu \\ 0 & 0 & 0 \\ \nu & 0 & 1 \end{bmatrix}\begin{Bmatrix} W_r d\bar{\varepsilon}^{\,p} + Q_r\,dT + d\varepsilon^s + \nu dp_g / E \\ \left(1-\nu^2\right)dp_g / E \\ W_z d\bar{\varepsilon}^{\,p} + Q_z\,dT + d\varepsilon^s + \nu dp_g / E \end{Bmatrix} \tag{11.2-35}$$

The singularity of $[C_{II}]$ reflects the fact that the radial displacements of the inner and outer radii of a cracked element cannot be determined uniquely from its exterior loads. This is due to the reason that a rigid body radial displacement of an element is a possibility. However, when all of the element stiffness matrices for an axial segment are assembled together, the resulting global stiffness matrix is, in general, non-singular and a unique solution for the displacements can be found.

11.2.2 Algorithm for Separating the Components of the Total Strain

In FPIN2, first the finite element equilibrium equations (described in Section 11.2.4.2) are solved to obtain the increments of total apparent strain. After separating the elastic contribution through the use of algorithm described below, we can then calculate the stresses from Eq. 11.2-11. The algorithm, which is based on a method developed by Schreyer [11-8], also yields the other components of the total strain. This

algorithm has been extended in FPIN2 to include crack strains, swelling strains, and more general constitutive laws. The algorithm can be broken into six steps as follows.

Step 1: At the beginning of a time step, t_i, all quantities of interest are assumed to be known. Approximations to the elastic strains at the end of time step, t_{i+1}, are calculated by subtracting the thermal strain (using new temperatures), estimated plastic strain, and the estimated swelling strain from the total strain:

$$\underline{\varepsilon}_N^e = \underline{\varepsilon}_{i+1}^t - \underline{\varepsilon}_{i+1}^{\Theta} - \underline{\varepsilon}_N^p - \varepsilon_N^s \tag{11.2-36}$$

Since the algorithm is iterative, an iteration counter, N, is introduced as a subscript. In FPIN2, starting values (N=1) for plastic strain are estimated using the values at the beginning of the time step and the previous plastic strain rate as follows

$$\underline{\varepsilon}_1^p = \underline{\varepsilon}_i^p + \frac{d\underline{\varepsilon}_i^p}{dt}\Delta t \tag{11.2-37}$$

Similarly, an initial estimate for the swelling strain is given by

$$\underline{\varepsilon}_1^s = \underline{\varepsilon}_i^s + \frac{d\underline{\varepsilon}_i^s}{dt}\Delta t \tag{11.2-38}$$

Step 2: The generalized Hooke's law is used to calculate the stresses:

$$\underline{\sigma}_N = [C]\underline{\varepsilon}_N^e \tag{11.2-39}$$

Step 3: The time rate-of-change of the equivalent plastic strain is calculated from

$$\frac{d\bar{\varepsilon}_N^p}{dt} = \frac{\bar{\varepsilon}_N^p - \bar{\varepsilon}_i^p}{\Delta t} \tag{11.2-40}$$

Similarly, the rate-of-change of the swelling strain is calculated from

$$\frac{d\varepsilon_N^s}{dt} = \frac{\varepsilon_N^s - \varepsilon_i^s}{\Delta t} \tag{11.2-41}$$

Step 4: Successive evaluations of the plastic flow condition $f_N\left(\sigma_{eN}, \bar{\varepsilon}_N^p, d\bar{\varepsilon}_N^p/dt, T_{i+1}\right)$ and the swelling function $g_N\left(\sigma_{mN}, \varepsilon_N^s, d\varepsilon_N^s/dt, T_{i+1}, \nabla T_{i+1}, \rho_N\right)$ are performed using equivalent and mean stresses that are calculated from

$$\sigma_{eN} = \sqrt{\frac{3}{2}\left(S_{rN}^2 + S_{\theta N}^2 + S_{zN}^2\right)} \tag{11.2-42}$$

$$\sigma_{mN} = \frac{\sigma_{rN} + \sigma_{\theta N} + \sigma_{zN}}{3} \tag{11.2-43}$$

Step 5: The increments in equivalent plastic strain and swelling strain are obtained from

$$\Delta\bar{\varepsilon}_N^p = -\frac{f_N}{df_N / d\bar{\varepsilon}^p} \tag{11.2-44}$$

$$\Delta\varepsilon_N^s = -\frac{g_N}{dg_N / d\varepsilon^s} \tag{11.2-45}$$

These expressions represent the correction term in the Newton-Raphson method that is applied to find the $\bar{\varepsilon}^p$ and ε^s that satisfy the constitutive equations, Eqs. 11.2-14 and 11.2-16. Experience indicates that convergence of the entire algorithm is enhanced if only a single Newton-Raphson correction is performed for each *N*. Differentiating the plastic flow condition f=0 with respect to $\bar{\varepsilon}^p$ and the swelling function g = 0 with respect to ε^s gives

$$\frac{df}{d\bar{\varepsilon}^p} = -3G\frac{\partial f}{\partial \sigma_e} + \frac{\partial f}{\partial \bar{\varepsilon}_p} + \frac{1}{\Delta t}\frac{\partial f}{\partial \dot{\bar{\varepsilon}}_p} \tag{11.2-46}$$

and

$$\frac{dg}{d\varepsilon^s} = -3K\frac{\partial g}{\partial \sigma_m} + \frac{\partial g}{\partial \varepsilon^s} + \frac{1}{\Delta t}\frac{\partial g}{\partial \dot{\varepsilon}^s} \tag{11.2-47}$$

where G is the shear modulus and K is the bulk modulus

$$G = \frac{E}{2(1+\nu)} \tag{11.2-48}$$

$$K = \frac{E}{3(1-2\nu)} \tag{11.2-49}$$

The total derivatives in Eqs. 11.2-46 and 11.2-47 are evaluated for fixed total strain at t_{i+1} (the details of these derivations can be found in pp. 23-25 of Ref. 11-2).

Step 6. The last step in the algorithm consists of calculating the new equivalent plastic strain:

$$\bar{\varepsilon}^p_{N+1} = \bar{\varepsilon}^p_N + \Delta\bar{\varepsilon}^p_N \tag{11.2-50}$$

and the new plastic strain increments by use of the associated flow rule:

$$\underline{\Delta\varepsilon}^p_N = \frac{3}{2\sigma_{eN}} \Delta\bar{\varepsilon}^p_N \left(\underline{\sigma}_N - \underline{\sigma}_{mN}\right) \tag{11.2-51}$$

and from them, the new plastic stains as follows

$$\bar{\varepsilon}^p_{N+1} = \underline{\varepsilon}^p_N + \underline{\Delta\varepsilon}^p_N \tag{11.2-52}$$

Similarly, the new swelling strains are calculated from

$$\bar{\varepsilon}^s_{N+1} = \underline{\varepsilon}^s_N + \Delta\varepsilon^s_N \tag{11.2-53}$$

It should be emphasized here that the increments in Eqs. 11.2-52 and 11.2-53 are added to the plastic and swelling strains corresponding to the last iterate, rather than to the strains corresponding to the beginning of the time step. Iteration continues through steps 1-6 until these increments, which are Newton-Raphson corrections to the strains, are acceptably small.

For a continuous (Type I) element, the total strain is equal to the apparent strain calculated from the equilibrium equations. Therefore, the total strain vector is known at the end of a time step. For Type II elements, existence of radial cracks requires modifications to the algorithm to obtain non-zero crack strain component, ε^e_θ. In Step 1, the component of the elastic strain not obtainable from Eq. 11.2-36, $\varepsilon^e_{\theta N}$, is calculated by substituting $-p_g$ for $\sigma_{\theta N}$ in Eq. 11.2-39 and solving this equation for $\varepsilon^e_{\theta N}$.

When the algorithm is converged, the elastic, plastic, and swelling components of the circumferential and/or axial strains are known for both element types at the end of the time step. Using these values, the total circumferential strain is calculated from

$$\varepsilon^t_{\theta,i+1} = \varepsilon^e_{\theta,i+1} + \varepsilon^p_{\theta,i+1} + \varepsilon^\Theta_{\theta,i+1} + \varepsilon^s_{\theta,i+1} \tag{11.2-54}$$

And finally, the crack strain is determined from the known "apparent total strain" as follows

$$\varepsilon^c_{\theta,i+1} = \varepsilon^t_{\theta,i+1} - \varepsilon^a_{\theta,i+1} \tag{11.2-55}$$

11.2.3 Continuous Cracking Model

If an element is uncracked in the θ plane, it is reasonable to assume that cracking will occur if the tensile stress σ_θ across that plane exceeds some fracture stress $\sigma_{\theta F}$. At that point, the element type will change to Type II and a non-zero crack strain ε^c_θ will begin to accumulate. If the crack is closed during the subsequent deformation, the element type will switch back to Type I which does not have cracks. However, consideration of the cracking/closure of the entire element at once may introduce large unphysical perturbations into the mechanical analysis that cause unrealistic results and difficulties with the convergence of the basic solution algorithm. This problem is avoided in FPIN2 by using a continuous cracking model [11-9].

If the tangential stress in the uncracked part of the element is assumed to have reached the fracture stress and the tangential stress across the cracked part of the element equals $-p_g$, the average tangential stress for the element is given by

$$\sigma_\theta = \sigma_{\theta F} + \left(\sigma_{\theta F} + p_g\right)\frac{\varepsilon^c_\theta}{\varepsilon^c_0} \tag{11.2-56}$$

where ε^c_0 is a positive constant. The crack penetration distance is assumed to be proportional to the average crack opening strain, ε^c_θ.[2] This continuous cracking equation produces a stress across the fracture surface of a finite element that varies smoothly from the fracture stress down to the gas pressure as the crack strain increases from zero to ε^c_0. Once ε^c_θ exceeds ε^c_0, it is assumed that the stress across the fracture surface remains equal to the gas pressure.

Although a one-dimensional analysis cannot represent the details of the two-dimensional stress field at the tips of actual cracks, it has been shown that the continuous cracking model used in FPIN2 can determine the stable growth of the radial cracks to a reasonable accuracy [11-10]. Incorporation of Eq. 11.2-56 into the mechanical analysis is straightforward, but it leads to somewhat lengthy expressions in relating the stresses to the strains for the cracked elements. The net result changes some of the equations in the algorithm described in Section 11.2.2 and the expressions in the element stiffness matrices as discussed Section 11.2.4.2.

11.2.4 Finite Element Formulation

In this section, the finite element method that is used to derive a set of algebraic equations governing the equilibrium of the fuel and cladding is described. The first step

[2] Because of the definition of crack strain in Eq. 11.2-7, $\underline{\epsilon}^c$ will be negative for opening of cracks. The crack strain input to and output from FPIN2 is the absolute value of this quantity.

in the derivation is the development of integral forms of the equilibrium equations or, in other words, the virtual work equations.

11.2.4.1 Virtual Work Equations

When all shear stresses are set to zero, the equations of equilibrium in cylindrical coordinates reduce to

$$\sigma_{r,r} + \frac{\sigma_r - \sigma_\theta}{r} = \frac{\sigma_{\theta,\theta}}{r} = \sigma_{z,z} = 0 \tag{11.2-57}$$

Since the circumferential displacements are either known to be zero or can be determined form algorithm described in Section 11.2.2, developing the virtual work equations for the circumferential displacements is not necessary. By multiplying the equilibrium equation in the r direction by an arbitrary function ϕ_r, and equation in the z direction by ϕ_z, and integrating the resulting sum over the ring shaped finite element, we get

$$\int_V \left[\left(\sigma_{r,r} + \frac{\sigma_r - \sigma_\phi}{r} \right) \phi_r + \sigma_{z,z}\, \phi_z \right] dV = 0 \tag{11.2-58}$$

Using the formula for the derivative of a product and applying the divergence theorem, Eq. 11.2-58 can be rewritten as

$$\begin{aligned} \int_V \left[\sigma_r \phi_{r,r} + \frac{\sigma_\theta \phi_r}{r} + \sigma_z \phi_{z,z} \right] dV &= \int_V \left[\frac{1}{r} \left(r \sigma_r \phi_r \right)_{,r} + \left(\sigma_z \phi_z \right)_{,z} \right] dV \\ &= \int_S \left[\sigma_r \phi_r \hat{i}_r + \sigma_z \phi_z \hat{i}_z \right] \cdot \hat{n}\, ds \end{aligned} \tag{11.2-59}$$

where $\hat{n}$ is the outward normal to the surface S of volume V, and $\hat{i}_r, \hat{i}_z$ are unit vectors in the r and z directions. Assuming that ϕ_z has the form

$$\phi_z = \psi z \tag{11.2-60}$$

in which ψ is an arbitrary constant, and also assuming that $\phi_r, \sigma_r, \sigma_\theta,$ and σ_z are all independent of z, Eq. 11.2-59 reduces to

$$\int_A \left[\sigma_r \phi_{r,r} + \frac{\sigma_\phi \phi_r}{r} + \sigma_z \psi \right] dA = \int_C \sigma_r \phi_r \hat{i}_r \cdot \hat{n}\, dC + \psi F \tag{11.2-61}$$

where A is the area of the intersection of the ring shaped finite element with the plane z = 0, and C is the curve bounding A. F describes the axial force.

A linear approximation is used for the finite-element displacement function, ϕ_r, appearing in the virtual work equations. For the one-dimensional element in Fig. 11.2-2, it is given by

$$\phi_r = u_1 N_1 + u_2 N_2 \tag{11.2-62}$$

where u_1 and u_2 are the radial displacements of nodes 1 and 2, and the shape functions are

$$N_1 = \frac{b-r}{l} \tag{11.2-63}$$

and

$$N_2 = \frac{r-a}{l} \tag{11.2-64}$$

Substituting Eq. 11.2-62 into the virtual work equation, Eq. 11.2-61, and integrating over the area of the element, A_e, we get[3]

$$\int_{A_e} [B]^T \underline{\sigma}\, dA = \{t_1, t_2, F\}^T \tag{11.2-65}$$

where $[B]$, t_1 and t_2 are defined as

$$[B] = \frac{1}{1}\begin{bmatrix} -1 & 1 & 0 \\ \left(\frac{b}{r}-1\right) & \left(1-\frac{a}{r}\right) & 0 \\ 0 & 0 & 1 \end{bmatrix} \tag{11.2-66}$$

$$t_i = \int_C \sigma_r N_i \hat{i}_r \cdot \hat{n}\, dC \quad (\text{i}=1,2). \tag{11.2-67}$$

[3] To define ϕ_r over the entire domain of the integration, A, we must cover the domain with a finite element mesh and then sum the contributions at each node from all elements sharing the node. For brevity, this finite element assembly process is not discussed here and formulation is developed for a single element only.

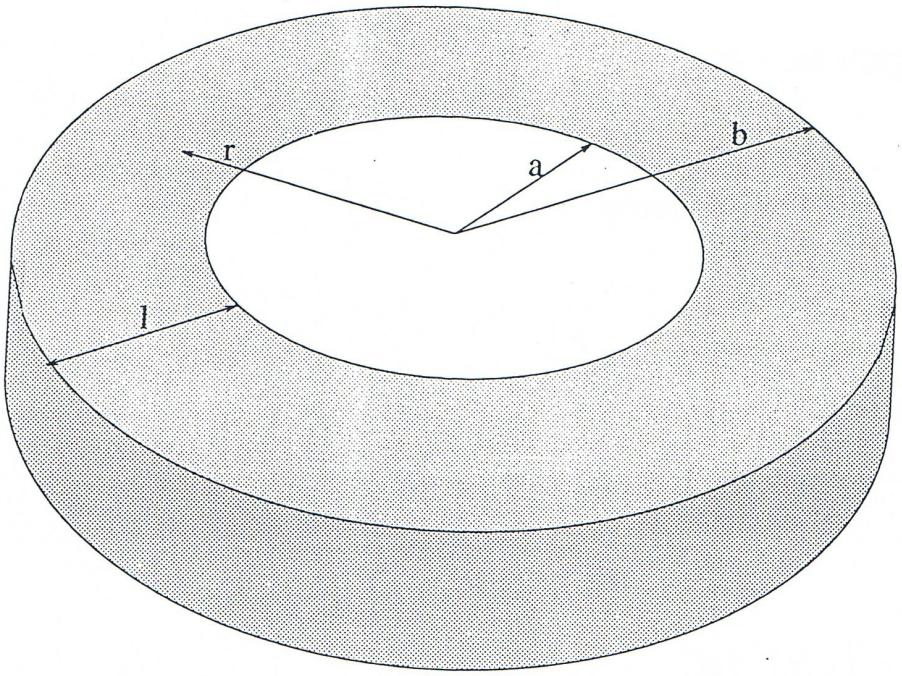

Fig. 11.2-2: Finite Element Cross Section

11.2.4.2 Incremental Form of the Virtual Work Equations

Eq. 11.2-65 can be viewed as expressing the balance between the external forces on the right hand side and the internal forces on the left hand side. The external forces are known functions of time. The stress field on the other hand must be found to satisfy the Eq. 11.2-65 and the constitutive laws for the material. Since the constitutive equations are, in general, highly non-linear, an incremental technique is used in FPIN2 based on iterations within each increment to calculate the stresses.

Assuming that all the stresses at time t_i are known, the equilibrium equation (Eq. 11.2-65) can be rewritten at the end of the time step, t_{i+1}, as

$$\underline{\Delta f}^{\text{int}} = \underline{\Delta f}^{ext} \tag{11.2-68}$$

where

$$\underline{\Delta f}^{\text{int}} = \underline{f}^{\text{int}}_{i+1} - \underline{f}^{\text{int}}_{i} = \int_{A_e} [B]^T \, \underline{\Delta\sigma} \, dA \tag{11.2-69}$$

and

$$\underline{\Delta f}^{ext} = \underline{f}_{i+1}^{ext} - \underline{f}_{i}^{ext} \tag{11.2-70}$$

The problem has now been reduced to finding the stress increments $\underline{\Delta\sigma}$ appearing implicitly in Eq. 11.2-68 through Eq. 11.2-69. These stress increments

$$\underline{\Delta\sigma} = \underline{\sigma}_{i+1} - \underline{\sigma}_{i} \tag{11.2-71}$$

are calculated through an iterative procedure.

As discussed in Section 11.2.1.5, the stress increments are approximated by Eq. 11.2-27 that is repeated here

$$\underline{\Delta\sigma} = \left[C\right]_i \underline{\Delta\varepsilon}^{a} - \underline{\Delta\sigma}_i^{ps} \tag{11.2-72}$$

where the elastic modulus, $[C]_i$, and pseudo-stress, $\underline{\Delta\sigma}_i^{ps}$, are evaluated using values at t_i (or at t_{i+1} if known). The apparent strain increment, $\underline{\Delta\varepsilon}^{a}$, in Eq. 11.2-72 can be expressed in terms of displacement increments through the strain-displacement relations, as discussed in Section 11.2.1.1. Using a similar representation with the virtual work functions, ϕ_r and ϕ_z, radial and axial displacement increments can be written as

$$\Delta u = \Delta u_1 N_1 + \Delta u_2 N_2 \tag{11.2-73}$$

$$\Delta w = z\Delta\psi \tag{11.2-74}$$

Using these in Eq. 11.2-8 leads to

$$\underline{\Delta\varepsilon}^{a} = \left[B\right]\underline{\Delta\delta} \tag{11.2-75}$$

where

$$\underline{\Delta\delta} = \left\{\Delta u_1, \Delta u_2, \Delta\psi\right\}^T \tag{11.2-76}$$

After substituting Eq. 11.2-75 into Eq. 11.2-72, and subsequently replacing the result in Eq. 11.2-69, we can rewrite the equilibrium equation, E. 11.2-68, in the form

$$\left[K\right]_i \underline{\Delta\delta} = \underline{\Delta f}^{ext} + \underline{\Delta f}_i^{ps} \tag{11.2-77}$$

where

$$[K]_i = \int_{A_e} [B]_i^T [C]_i [B]_i \, dA \tag{11.2-78}$$

and

$$\underline{\Delta f}_i^{ps} = \int_{A_e} [B]_i^T \, \underline{\Delta \sigma}_i^{ps} \, dA \tag{11.2-79}$$

Here $[K]_i$ is the stiffness matrix evaluated at t_i using the known values. It should be noted that the forms of the matrices $[C]$ and $[B]$ in Eq. 11.2-78 and $\underline{\Delta \sigma}^{ps}$ in Eq. 11.2-70 depend on the type of element considered as discussed earlier in Section 11.2.1.5. Explicit formulas for the stiffness matrix and load vectors for both element types considered are given in Appendix 11.1.

11.2.4.3 Iterative Solution of the Equilibrium Equations

Eq. 11.2-77 is the incremental form of the virtual work (or equilibrium) equation. Since the stiffness matrix $[K]_i$ is known, it constitutes a set of linear equations that can be solved for the displacement increments, $\underline{\Delta \delta}$. Eq. 11.2-75 then gives the increment in apparent total strain, $\underline{\Delta \varepsilon^a}$, and the algorithm described in Section 11.2.2 gives the stresses at time t_{i+1}. These stresses, in turn, can be used in Eq. 11.2-69 to calculate the internal force vector. However, since the expression for the stress increment in Eq. 11.2-72 is only approximate, the equilibrium equation (Eq. 11.2-68) will not be satisfied in general.

In FPIN2, another iterative procedure is used to ensure that the stress estimates satisfy the equilibrium equation to an acceptable degree of accuracy. By defining the residual, or the error, in Eq. 11.2-68 as follows

$$\underline{r} = \underline{f}_{i+1}^{ext} - \underline{f}_{i+1}^{\text{int}} \tag{11.2-80}$$

The successive evaluations of the nodal variable increments, $\underline{\Delta \delta}$, are calculated from

$$(K)_i \, \underline{\Delta \delta}_j = \underline{\Delta f}^{ext} + \underline{\Delta f}_i^{ps} + \underline{r}_{j-1} \tag{11.2-81}$$

where j is the iteration index.

The convergence of this iterative scheme is monitored through the norm of the residual vector. If this error is sufficiently small, then the equilibrium equations are assumed to be satisfied and the computation is advanced to the next time step. Otherwise, the new residual vector $\underline{r}_j$, is calculated and added to the right hand side of Eq. 11.2-81 (the previous residual vector, $\underline{r}_{i+1}$, remains there as well). Fig. 11.2-3 summarizes this algorithm for iterative solution of the equilibrium equations.

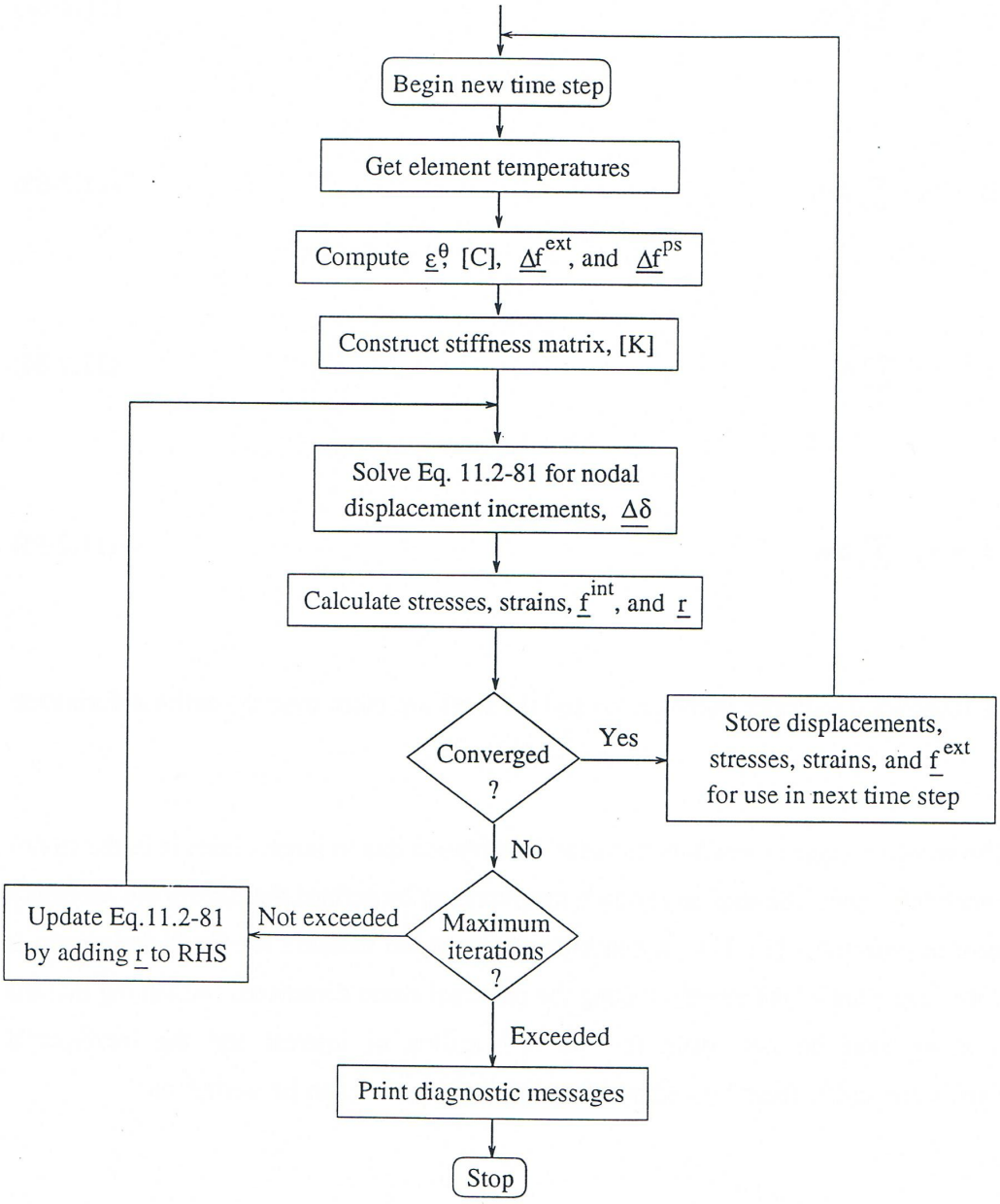

Fig. 11.2-3: Iterative Solution of Equilibrium Equations

11.2.5 Large Strain Analysis

Since fuel pin deformation at high temperatures may involve large plastic strains as well as massive local swelling, it is important that the formation of the mechanics model allows for analysis of large strains. Consideration of large strains has impacts on the equilibrium equations derived in Section 11.2.4 and the strain-displacement definitions given in Section 11.2.1. Both changes involve straightforward modifications of the incremental (small perturbation) analysis that has already been derived.

Since the stresses at any time t_{i+1} must satisfy the equilibrium equations (Eq. 11.2-57) in the deformed cylindrical geometry, the virtual work equations should be applied to the fuel element geometry at t_{i+1} rather than the initial geometry as assumed previously. Following through the derivation of the finite-element equilibrium equation (Eq. 11.2-65), it is easy to show that the only change necessary to accommodate large strains is to redefine the geometric variables to refer to the deformed element. Furthermore, if the incremental deformation between times t_i and t_{i+1} is small, negligible error will be incurred by replacing the geometric variables at t_{i+1} by these values at t_i. These values are readily available form the initial undeformed geometry and the known deformation. From Eqs. 11.2-73 and 11.2-74 for instance, we have

$$a = a_0 + \sum_i \Delta u_1 \tag{11.2-82}$$

$$b = b_0 + \sum_i \Delta u_2 \tag{11.2-83}$$

$$r = r_0 + \sum_i \Delta u \tag{11.2-84}$$

$$z = z_0 + \sum_i \Delta w \tag{11.2-85}$$

where the subscript 0 indicates the initial values, and the sums are taken over the entire deformation history.

The second change in small-perturbation formulation due to large strains is in the strain-displacement definitions. Several large strain measures can be defined that satisfy the necessary requirement of objectivity [11-11]. A convenient large strain measure for the fuel elements is given by the logarithm of the stretches along the principal strain directions. Assuming that the principal strain axes do not rotate for the deformation of interest and the incremental displacements are small, these logarithmic large strain measures can be written as

$$\varepsilon_{r,i+1}^{t} = \varepsilon_{r,i}^{t} + \frac{\partial}{\partial r_i}(\Delta u) \tag{11.2-86a}$$

$$\varepsilon_{\theta,i+1}^{t} = \varepsilon_{\theta,i}^{t} + \frac{\Delta u}{r_i} \tag{11.2-86b}$$

$$\varepsilon_{z,i+1}^{t} = \varepsilon_{z,i}^{t} + \frac{\partial}{\partial z_i}(\Delta w) \tag{11.2-86c}$$

Comparing Eqs. 11.2-86 with Eq. 11.2-5 shows that, in order to use the logarithmic large strain measure, the only change necessary in the analysis given previously is to use the displacement increments to calculate the strain increments and then to determine total strains by adding the increments throughout the deformation history.

11.3 Metal Fuel Element Models

Although the FPIN2 code was originally developed for the purpose of analyzing oxide fuels, it has been modified for the analysis of metallic fuels. The metal fuel version of the code includes numerous improvements to the basic mechanical analysis models that reflect the experience gained from the in-pile TREAT tests on EBR-II irradiated prototypic fuel of the IFR concept. In addition, models for molten cavity formation, the large gas plenum, molten fuel extrusion, and fuel-cladding eutectic formation are provided to complement the fuel element mechanics calculation.

There are many differences between metal and oxide fuels that affect the transient response of the fuel elements. The existence of a large fission gas plenum in metal-alloy fueled elements plays a major role in determining the internal pin pressure during a transient. The sodium bond and comparatively large radial fuel-cladding gap requires consideration of expelling sodium into the plenum as the fuel expands and the gap closes. Metal fuel thermal conductivity is an order of magnitude larger than oxide fuel, and that leads to a flatter radial temperature profile and a more rapid spreading of the region of molten fuel. Since the metal fuel solidus temperature is well below the cladding melting temperature, in many cases fuel can be expected to melt entirely before the cladding fails. Due to the high fuel thermal conductivity, melting usually begins at or near the top of the fuel column with the axial profile of the fuel centerline temperature more closely following the coolant temperature profile than that for oxide fuel. This prevents large cavity pressurization effects in metallic fuels. In addition, a low melting temperature eutectic alloy is expected to form in metallic fuels between the fuel and cladding at temperatures below the anticipated cladding failure. This eutectic formation allows the fuel and cladding to slip freely in the axial direction and can lead to an accelerated cladding failure at elevated temperatures. Cracking is not a significant phenomenon in metallic fuel pins, but metal fuel swelling can be important.

The current version of the FPIN2 coupled with SASSYS/SAS4A includes various model modifications and additions that address these differences between oxide and metal fuels. The following sections contain discussions of these additions and modifications made to FPIN2 for the analysis of metal-fueled elements. The most significant extension to the code is the inclusion of a model for the plenum region above the fuel column as discussed in Section 11.3.1. Extrusion of molten fuel into the plenum as an additional axial expansion mechanism is discussed in Section 11.3.2. Basic mechanical properties of metal-alloy fueled elements are outlined in Section 11.3.3. The constitutive equations for fuel creep and a non-equilibrium approximation to fuel swelling are presented in Section 11.3.4 and Section 11.3.5, respectively. The plastic flow behavior of three types of cladding materials commonly used in metallic fuel elements of the IFR concept is discussed in Section 11.3.6. Fuel-cladding eutectic formation and its impact on the mechanical analysis of fuel elements are summarized in Section 11.3.7. And finally, the fuel element failure formulation is outlined in Section 11.3.8.

11.3.1 Central Cavity and Plenum Models

Internal pin pressure is calculated in FPIN2 using straightforward volume accounting models of the central cavity and the gas plenum. The radial boundary of the cavity for each axial segment is assumed to be at the point where the fuel has reached the solidus temperature. Elements inside the cavity boundary are assumed to be in a hydrostatic state of stress equal to the cavity pressure and are dropped out of stress-strain calculation. These elements occupy a volume in proportion to their density and contribute to the volume and mass balance iteration that determines the cavity pressure.

Metallic fuel elements lead to relatively low transient induced internal pin pressure since (1) fuel porosity easily accommodates the fuel volume expansion upon melting, (2) fuel melting begins at or near the top of fuel column, and (3) metallic fuels have less restrictive flow path for fission gas passage to the plenum. Thus, the large gas plenum is very effective in mitigating any large pressure buildup inside the fuel elements. The pin plenum model of FPIN2 is based on the following assumptions:

1. The internal pin pressure, p_g, is considered uniform throughout the interior of a metallic fuel element.
2. The plenum region is assumed to be at the uniform temperature.[4]
3. The thermal expansion of the fill sodium and its expulsion from the fuel-cladding gap as the gap closes is accounted for. However, sodium compressibility is assumed to be negligible at the expected pressure range.

The first level of iteration, or outer loop, in the mechanical analysis section of the FPIN2 is the search for the internal pin pressure p_g. According to the calculation

[4] In stand-alone FPIN2 calculation, this plenum temperature is assumed to be equal to the coolant outlet temperature.

sequence, the temperatures of the cavity and plenum materials are known at the beginning of a new time step before the pin pressure is found. Using these temperatures, the following can be calculated:

1. Cavity boundary changes due to fuel melting,
2. Mass of the gas in the cavity, including the gas released upon melting,
3. Mass-average temperature of the gas in the cavity,
4. Volume available from porosity released after fuel melting,
5. The thermal expansion of the sodium in the plenum.

The algorithm for calculating the plenum and cavity pressures are outlined below for the case where the two volumes are connected and share a common pressure, p_g. The pin pressure, p_g, is calculated by considering the two relationships between the gas volume and pressure that must be satisfied: the ideal gas law, and the interaction between pressure and cavity boundary displacements. Pin molten-cavity and plenum gases are considered as separate entities with individual compositions and temperatures. Since the masses of the gases in the cavity, m_g^C, and the plenum, m_g^P, as well as the temperatures of the cavity gas, T_g^C, and the plenum gas, T_g^P, are known, the ideal gas law reduces to an inverse relationship between the total gas volume, V_g^{IGL}, and the pressure as follows

$$V_g^{IGL} = \frac{m_g^C R^C T_g^C + m_g^P R^P T_g^P}{p_g} \tag{11.3-1}$$

where R^C and R^P are the gas constants for cavity and plenum gases, respectively. The second relationship involves the geometrical calculation of the volume available to the gas that depends on displacement of the solid fuel, cladding, and plenum tube. The liquid fuel and sodium are assumed to be incompressible. Since the gas in the cavity and plenum are considered separately, the total volume has two components

$$V_g^{MECH}\left(p_g\right) = V_g^C\left(p_g\right) + V_g^P\left(p_g\right) \tag{11.3-2}$$

where V_g^C is the available cavity volume that is calculated using the finite element analysis of solid fuel and cladding, and V_g^P is the volume available for the gas in the plenum. A negative value of V_g^C means that the molten fuel material is extruded upward into the plenum.

The two values for the total volume, V_g^{IGL} and V_g^{MECH}, are equal when the correct value of p_g is found. In FPIN2, Newton's method is used to fine the value of p_g such that

$$f\left(p_g\right) = V_g^{IGL} - V_g^{MECH} = 0 \tag{11.3-3}$$

The Newton iteration equation

$$p_g^{i+1} = p_g^i - \frac{f\left(p_g^i\right)}{f'\left(p_g^i\right)} \tag{11.3-4}$$

requires the derivative of V_g^{IGL} and V_g^{MECH} with respect to p_g (i is the iteration counter). The derivative of V_g^{IGL} is easily calculated from the ideal gas law and the derivative of V_g^{MECH} is found by forming a finite difference quotient from two calculations of V_g^{MECH} at two neighboring values of p_g.

The total mass of sodium, m_{Na}^T, and mass of the gas in the plenum, m_g^P, are obtained from the initial conditions. The inventory of sodium within the fuel element consists of sodium in the fuel-cladding gap, m_{Na}^G, and in the plenum, m_{Na}^P :

$$m_{Na}^T = m_{Na}^P + m_{Na}^G \tag{11.3-5}$$

where

$$m_{Na}^P = \rho_{Na}\left(T^P\right)\pi\, r_P^2\, h_{Na}^P \tag{11.3-6}$$

$$m_{Na}^G = \sum_j \rho_{Na}\left(T_j\right)\pi\left(r_{ci}^2 - r_{fo}^2\right)_j \Delta z_j \tag{11.3-7}$$

The symbols in Eqs. 11.3-6 and 11.3-7 are defined as follows:

ρ_{Na} = sodium density,

T^P = plenum temperature,

r_p = cladding inner radius in plenum region,

h_{NA}^P = height of sodium column in plenum,

r_{ci} = cladding inner radius for axial segment j,

r_{fo} = fuel outer radius for axial segment j,

Δz_j = height of fuel axial segment j.

The mass of the plenum gas is determined by using the ideal gas law:

$$m_g^P = \frac{P^P \pi r_P^2 \left(h^P - h_{Na}^P\right)}{R^P T^P} \tag{11.3-8}$$

where P^P is the plenum pressure and h^P is initial plenum height. The plenum pressure is obtained from a user specified reference pressure at a reference temperature as follows

$$P^P = P_{ref} \frac{T^P}{T_{ref}} \tag{11.3-9}$$

During the transient analysis, the cavity pressure algorithm requires the volume in the plenum available to the plenum fission gas and to the material extruded from the molten cavity. This value is calculated by subtracting the volume of the sodium in the plenum from the total volume of the deformed plenum tube. Thus,

$$V_g^P = V^P - V_{Na}^P \tag{11.3-10}$$

The total plenum volume, V^P, is found by assuming that the plenum tube can be treated as a thermoelastic thin shell. The volume of sodium in the plenum is found using the equation

$$V_{Na}^P = \frac{m_{Na}^T - m_{Na}^G}{\rho_{Na}\left(T^P\right)} \tag{11.3-11}$$

11.3.2 Extrusion of Molten Fuel into the Plenum

The procedure in FPIN2 for calculating the behavior of the molten cavity materials uses a simple hydrostatic model based on volume accounting. As discussed in previous section, a volume and mass balance iteration determines the cavity pressure. For transients in which initial fuel melting is observed below the fuel-plenum interface, plenum and cavity pressure equations are solved separately, leading generally to a cavity pressure larger than the plenum pressure. Once melting reaches the top axial segment, the two pressures eventually equilibrate to give a common pin pressure. The temporary imbalance between the cavity and plenum pressures plays an important role in the dynamics of the molten fuel extruded into the plenum.

The extrusion of the molten cavity material into the plenum is calculated at the completion of the pressure iteration and consists of calculating the excess volume of the cavity materials over the volume available in the molten cavity. Both the radial and axial dimensions of the cavity section for each axial segment are based on the deformed geometry. The materials in the cavity include liquid fuel at a temperature above the liquidus temperature, solid fuel at a temperature between the solidus and liquidus, and the fission gas that is assumed to obey the ideal gas law and is released to the cavity in

proportion to the melt fraction. Open porosity is available to the fission gas volume when the fuel reaches the solidus temperature, but closed grain boundary porosity is release d in proportion to the metal fraction.

For low-burnup fuel pins, the bond sodium in the fuel-cladding radial gap affects the extrusion of molten fuel into the plenum. The metallic fuel can melt completely across the fuel radial cross section in an axial segment. Although the large gap in fresh metallic fuels is not expected to close by the time of 100% fuel melting, the bond sodium in the gap is expected to escape into the plenum as the molten fuel slumps to fill up the gap due to the large density difference between fuel and sodium. This local slumping lessens the fuel extrusion; however, metal fuels at as low as 0.35 at.% burnup contain sufficient fission gas to result in net upward axial fuel motion [11-12]. Two options are provided in FPIN2 to model this behavior. The first option is to assume that the fuel does not slump and expel the bond sodium. In this case, the fuel outer boundary is assumed to remain at the position it was in at the time of 100% melting. The second (default) option allows the molten fuel to move out to the cladding, with the bond sodium being expelled into the plenum and the gap volume being added to the molten cavity.

To handle the second option, a gap closure model has been added to move the molten fuel out to the cladding over several time steps as the bond sodium is expelled into the plenum and the gap volume becomes available to the molten cavity materials. In order to maintain the stability of the numerical calculation, a varying closure rate is coded in FPIN2 in which the fraction of the gap closed per time step is specified. Somewhat artificial time step dependence of this transition is necessary because the temperature drop across the gap may be as large as 30K. Since the radial temperature profile across the fuel element is relatively flat, an excessively rapid reduction of the gap ΔT may cause computational difficulties such as fuel refreezing during a power rise.

11.3.3 Basic Metal Fuel Properties

Thermal Properties: In the interfaced mode, the SAS-FPIN2 integrated model uses SASSYS/SAS4A routines to calculate fuel and cladding thermal material properties as discussed in Chapter 10. In the stand-alone mode, FPIN2 uses its own built-in correlations for metallic IFR fuel that have been developed by the "Metallic Fuel Properties Working Group" [11-12]. Melting related properties for the metallic fuels such as solidus and liquidus temperatures, heat of fusion, and volume change on melting are calculated using identical algorithms in FPIN 2 and SASSYS/SAS4A.

Elastic Properties: Tensile test data at room temperature for uranium and its alloys indicate yielding at very low stresses. The equation used in FPIN2 code for the Young's modulus is as follows

$$E = 0.12 \cdot 10^{6} \left(1 - 1.2\,p\right)\left(1 - 0.754 \cdot 10^{-3}\left(T - 588\right)\right) \qquad (11.3\text{-}12)$$

where E is Young's modulus (in Bars), p is fractional porosity, and T is temperature (K). This equation gives a value of one-tenth the handbook [11-7] value and should more properly be called a tangent modulus. However, for the expected monotonic loading of

most FPIN2 calculations, the fuel is treated as a pseudo-elastic-plastic material with plastic straining handled as secondary creep and yielding is included as part of the "elastic" behavior. In the code, Poisson's ratio is calculated from

$$\nu = 0.27\left(1-0.8p\right)\left(1+0.854\cdot 10^{-3}\left(T-588\right)\right) \tag{11.3-13}$$

where ν is Poisson's ratio, p is fractional porosity, and T is temperature (K).

Linear Thermal Expansion: In the metal fuel version of FPIN2, the thermal expansion is expressed in terms of handbook linear thermal expansion data, $\Delta L/L_0$ [11-7]. Using the data rather than the coefficient of thermal expansion, α, results in a more accurate accounting of the total expansion from room temperature to melting since it automatically includes the expansion at solid-to-solid phase transitions. The thermal expansion data and phase transition expansions have been approximated in the code as three straight line segments with breaks at the two solid-to-solid phase change temperature associated with the beginning and ending of the transformation to pure γ phase solid solution. The equations used for the binary fuel are

$$\frac{\Delta L}{L_0} = \begin{cases} 1.695\cdot 10^{-5}\left(T-293\right) & T<900 \\ 0.0103+7\cdot 10^{-5}\left(T-900\right) & 900<T<1000 \\ 0.0173+2.12\cdot 10^{-5}\left(T-1000\right) & T>1000 \end{cases} \tag{11.3-14}$$

And, the equations for the ternary fuel are

$$\frac{\Delta L}{L_0} = \begin{cases} 1.67\cdot 10^{-5}\left(T-293\right) & T<864 \\ 0.0095+6.7\cdot 10^{-5}\left(T-864\right) & 864<T<950 \\ 0.0153+2.12\cdot 10^{-5}\left(T-950\right) & T>950 \end{cases} \tag{11.3-15}$$

where and T is the temperature (K).

11.3.4 Secondary Creep of Metallic Fuels

Uranium alloys deform plastically under constant load at elevated temperatures. The secondary, or minimum, creep rate is defined as the steady-state rate that is attained under these conditions. The equations added to FPIN2 for metal fuels are obtained from a review of the data and theory for modeling secondary creep of U-Pu-Zr alloys that are of interest to the IFR concept [11-13]. Application of creep data to fuel pin analysis often requires correlating the data using mathematical functions of the governing variables. Such correlations range from purely empirical equations to theoretical equations involving fundamental physical properties. In FPIN2, and intermediate approach is preferred where theoretical models are used to obtain the form of the equation, but the parameters are determined form the creep data rather than the fundamental properties. Such an approach allows an interpolation of the data and gives reasonable confidence in often-required extrapolations beyond the database.

The particular form of the secondary creep equation used in FPIN2 is the form used to represent creep of UO_2 [11-12]. The total plastic strain rate, $\dot{\varepsilon}$, is given by

$$\dot{\varepsilon} = C_1\left(\dot{F},d\right)\sigma e^{\left(-\frac{Q}{RT}\right)} + C_2\left(\dot{F}\right)\sigma^n \exp^{\left(-\frac{Q}{RT}\right)} + C_3\left(T\right)\sigma\dot{F} \qquad (11.3\text{-}16)$$

where

$\dot{\varepsilon}$ = secondary creep rate, s^{-1}

σ = equivalent stress, MPa

R = universal gas constant, (1.987 cal/g-mole-K)

T = temperature, K

Q = activation energy, (cal/g-mole)

d = grain size, μm

$\dot{F}$ = fission rate, (fissions/cm^3-s)

C = material functions.

In Eq. 11.3-16, the first term represents diffusional creep, the second term dislocation creep, and the third fission-induced creep. Here, the low temperature deformation mechanisms are neglected such as dislocation glide and twinning that may occur in α uranium at temperatures less than 675K. On the other hand, the expected dependence of in-reactor creep on the fission rate is considered.

Some of the parameters in Eq. 11.3-16 are estimated from knowledge of the structure of material and the values that these parameters take for similar materials. At low temperatures, it is reasonable to postulate that the creep deformation of uranium alloys is dominated by the deformation of the α uranium matrix. This is particularly true if the other phases present are coarsely dispersed. When the α uranium matrix deformation is dominant, the activation energy is expected to be the self-diffusion energy in α uranium. The creep activation energy Q=52000 cal/g-mole has been determined experimentally for α uranium. It is shown that the temperature dependence of creep can be deduced using such a single activation energy and that the value of n=4.5 is appropriate in the high stress range [11-13]. Using these values for Q and n, C_1 and C_2 in Eq. 11.3-16 are chosen to minimize the least squares error between the calculated and measures values of log(z) where z is the Zener-Holloman parameter

$$z = \dot{\varepsilon} e^{\frac{Q}{RT}} \qquad (11.3\text{-}17)$$

The result is

$$C_1 = 0.5 \cdot 10^4 \ MPa^{-1} s^{-1}$$
$$C_2 = 6.0 \qquad MPa^{-1} s^{-1} \tag{11.3-18}$$

When the calculated time to 2% strain using these values is compared to data from creep tests of U-Pu-Zr alloys, results are found to be in acceptable agreement. Examination of experimental data suggests that the grain-size dependence of C_1 can be included as

$$C_1 = \left(\frac{160}{d}\right)^2 0.5 \cdot 10^4 \ MPa^{-1} s^{-1} \tag{11.3-19}$$

for grain sizes near 160 μm.

At temperatures above about 900K, the structure of the U-Pu-Zr alloys no longer contains an α uranium matrix. The transformations between 900K and 975K are complex and depend strongly on composition. Beyond 975K, however, the solid phase consists of a solid solution of uranium, plutonium, and zirconium over a wide range of compositions. In FPIN2, it is assumed that the creep rate in the intermediate temperature range falls between the creep rate of α uranium and solid solution γ phase. It is also assumed that creep of uranium alloys is governed by dislocation glide in the γ regime. The phenomenological creep equation is of the form

$$\dot{\varepsilon} = C_4 \sigma^3 e^{\left(-\frac{Q_\gamma}{RT}\right)} \tag{11.3-20}$$

where Q_γ is the creep activation energy in the γ phase, and the parameter C_4 is, in general, a function of composition and fission rate. Based on tracer diffusion data and/or additional creep data, Q_γ is approximated as the activation energy for creep of the pure γ uranium solvent

$$Q_\gamma = 28500 \text{ cal/g-mole} \tag{11.3-21}$$

The constant C_4 is chosen to fit data at 973K as

$$C_4 = 8.0 \ \cdot \ 10^{-2} \ MPa^{-3} \ s^{-1} \tag{11.3-22}$$

Since the data is somewhat limited and the Eqs. 11.3-16 and 11.3-20 are consistent with the creep of alloys with a high percentage of uranium, FPIN2 uses these expressions for all metal fuels.

Experience with earlier versions of the FPIN2 reveals that the evaluation of Eqs. 11.3-16 and 11.3-20 uses a substantial fraction of the computing time. Since the terms involving the exponential function depend only on the temperature, in the current

version such terms are evaluated only at the beginning of the mechanics calculation. Therefore, Eq. 11.3-16 is coded in the following form

$$\dot{\varepsilon} = \sigma\left(A + B\sigma^{n-1}\right) \tag{11.3-23}$$

where A and B are previously evaluated constants.

The creep equations given above are the same as those given in the Metallic Fuels Handbook [11-7]. However, fission-induced creep term is not included in the FPIN2 because it does not contribute significantly to the fuel stains on the time scale of the transients that the code has been designed to analyze.

11.3.5 Fission Induced Gas Swelling of Metal Fuels

Irradiated metal fuels experience rapid, large-scale swelling when subjected to overheating. From the safety perspective, this transient swelling could provide an inherent, self-limiting, negative reactivity feedback mechanism. In FPIN2, a transient swelling model has been incorporated to get an estimate for the magnitude of this fission-gas-induced swelling. This non-equilibrium model is based on diffusive growth of grain boundary bubbles.[5]

The distribution of fission gas retained in the fuel matrix is specified as input in FPIN2, and the remainder of the gas is assumed to be in solution or in small bubbles within the fuel grains. Fission gas that is retained in the fuel during steady-state irradiation provides a source for expansion of both solid and liquid fuel during overheating. The amount of gas in the pin plenum is also important since the plenum pressure is a major contributor to cladding loading and, therefore, cladding failure.

The following assumptions are the basis of the transient swelling model of FPIN2 for the analysis of the metallic fuels:

1. All “retained gas” (as measured from experiments on small samples of irradiated fuel) is in solution within the fuel or in the form of small bubbles within the fuel grains or on the grain boundaries.
2. A certain fraction of this gas (input parameter) is contained in grain boundary bubbles, fixed in number and all of the same initial radius (0.1 microns).
3. The open porosity contains fission gas in equilibrium with the plenum pressure.
4. Only the grain boundary bubbles contribute to the swelling of solid fuel.

In order to use this model, a relationship between the swelling strain, ε^s, the mean stress, σ_m, and the fuel temperature, T, is required as explained in Section 11.2.1.2.3. Studies on gas-bubbles growth mechanisms in metallic fuels indicate [11-14] that the transient fuel swelling is dominated by diffusive growth of grain boundary bubbles that is given by

[5] FPIN2 also provides an equilibrium swelling model as an option.

$$\frac{dr}{dt} = \frac{\Omega D_{gb} w \sin^3 \theta}{2kT r^2 L \eta} \phi \tag{11.3-24}$$

where

r = bubble radius in the grain boundary,

D_{gb} = grain boundary diffusion coefficient,

w = the boundary thickness,

Ω = the atomic (or molecular) volume, and

kT = thermal energy.

The overpressure, ϕ, in Eq. 11.3-24 is defined as

$$\phi = p_g + \sigma_m - \frac{2\gamma}{\rho} \tag{11.3-25}$$

and it represents the excess of gas pressure, p_g, over the sum of the mean stress, σ_m, and the surface tension restraint. This restraint is defined in terms of the specific surface free energy, γ, and the radius of curvature, ρ. For the grain-boundary bubbles,

$$\rho = \frac{r}{\sin\theta} \tag{11.3-26}$$

where θ is the intersection angle between the bubble surface and the grain boundary. In FPIN2, the fuel swelling rate is determined from Eq. 11.3-24 for the bubble growth rate and from the assumed bubble density.

The remaining constants in the above equations are geometric constants related to the bubble volume and the bubble spacing [11-14]. The gas in the bubbles is assumed to satisfy the ideal gas law so that

$$p_g = \frac{mRT}{V_b} \tag{11.3-27}$$

where m is the fixed mass of the gas per bubble and V_b is the volume of the bubbles. The mass of the gas in a bubble is determined by using the equilibrium conditions at the pretransient time when the bubble radius is assumed to be r_o. Thus

$$m = \frac{V_{bo}}{RT_o}\left(-\sigma_{mo} + \frac{2\gamma}{r_o}\right) \tag{11.3-28}$$

Since all of the grain boundary gas is assumed to reside in the closed porosity bubbles, the number density of bubbles, N, is given by

$$N = \frac{F_g}{m} \tag{11.3-29}$$

where F_g is the grain boundary fission gas density with units of g per cm^3 of fuel. For this simple model, only the swelling of the grain boundary bubbles is considered so that

$$\varepsilon^s = \frac{1}{3}\left(\frac{\Delta V}{V_o}\right) = \frac{1}{3} N\left(V_b - V_{bo}\right) \tag{11.3-30}$$

These equations, when combined, give the complete specification of the transient swelling model in the form

$$g\left(\varepsilon^s, \sigma_m, T\right) = 0 \tag{11.3-31}$$

The treatment of this constitutive equation for swelling in finite element mechanics is discussed in Section 12.2.2.

11.3.6 Generalized Plastic Flow Behavior of Cladding Materials

The tensile properties of the cladding materials (HT9, D9, and Type 316 stainless steel) are not frequently used in analyses of fuel element performance during normal operation, as designs are usually such that stresses imposed do not challenge the points where yielding should occur. However, under transient conditions at elevated temperatures the applied stresses can result in general yielding. This behavior is modeled in FPIN2 by using a unified plastic deformation model that includes both rate-independent deformation (classical plasticity) and rate-dependent deformation (creep). The equations describing the generalized plastic flow behavior of Type 316 stainless steel, D9, and HT9 cladding are presented in the following sections. The yield strength and ultimate strength of the materials can be calculated from the plastic flow equations by applying them to the geometry of a tensile test.

11.3.6.1 Type 316 SS and D9 Cladding

The deformation behavior of Type 316 stainless steel and D9 cladding can be described over a broad range of temperature and strain-rate with the set of equations shown below. These equations are used in calculations of the strength and deformation at temperatures ranging from room temperature to 1675 K under a variety of loading conditions. In this formalism, the true equivalent flow stress, σ_e, is described by the equation

$$\sigma_e = \sigma_s - (\sigma_s - \sigma_l)\exp\left(-\frac{\hat{\varepsilon}}{\varepsilon^*}\right) \tag{11.3-32}$$

where σ_l is yield stress of fully annealed unirradiated material, and σ_s is the saturation value of the flow stress that is asymptotically approached at large values of plastic strain. Ongoing true plastic strain is incorporated in the "hardness" parameter, $\hat{\varepsilon}$ (input in the model), as this strain is accumulated. The hardness parameter also contains contributions from prior cold work, irradiation hardening, and softening caused by annealing, all scaled as true plastic strain. Consequently, $\hat{\varepsilon} = 0$ for the fully annealed unirradiated material, and $\hat{\varepsilon} = 0.223$ for 20% cold-worked material (default value in the code). Finally, the value of the parameter ε^* is determined by the initial hardening rate θ_l of fully annealed material $(\hat{\varepsilon} = 0)$ which is given by

$$\theta_l = \frac{\sigma_s - \sigma_l}{\varepsilon^*} \tag{11.3-33}$$

The initial hardening rate, θ_l, is found to be only temperature dependent through the shear modulus; so, the rate and temperature dependencies of ε^* is obtained from the above equation.

The yield stress and saturation flow stress are rate and temperature dependent in accordance with the equations

$$\frac{\sigma_s}{G} = \frac{\sigma_{so}}{G}\left[1 - \exp\left(-\left(\frac{\dot{\varepsilon}_p}{\dot{\varepsilon}_{os}}\right)^{mK}\right)\right]^{1/K} \tag{11.3-34}$$

$$\frac{\sigma_l}{G} = \frac{\sigma_{lo}}{G}\left[1 - \exp\left(-\left(\frac{\dot{\varepsilon}_p}{\dot{\varepsilon}_{ol}}\right)^{mK}\right)\right]^{1/K} \tag{11.3-35}$$

where G is the temperature dependent shear modulus, $\dot{\varepsilon}_p$ is the equivalent plastic strain rate (the $d\bar{\varepsilon}^p/\mathrm{dt}$ term in Eq. 11.2-26), m and K are constants, and σ_{so}, σ_{lo}, $\dot{\varepsilon}_{os}$ and $\dot{\varepsilon}_{ol}$ are temperature dependent functions. The constant m is the rate sensitivity (the reciprocal of the stress-exponent n in a power-law creep equation), and K is a non-physical fitting parameter that governs the sharpness of the transition between rate-dependent flow and rate-independent flow. At a given temperature, in the high strain-rate limit, the equation for the saturation stress reduces to

$$\frac{\sigma_s}{G} = \frac{\sigma_{so}}{G} \tag{11.3-36}$$

whereas in the low strain-rate limit, it becomes

$$\frac{\sigma_s}{G} = \frac{\sigma_{so}}{G}\left(\frac{\dot{\varepsilon}_p}{\dot{\varepsilon}_{os}}\right)^m \tag{11.3-37}$$

which reflects the typical power-law creep behavior observed for these materials at high temperatures and low strain rates. The equation for the yield stress behaves similarly. The temperature dependencies of σ_{so} and σ_{lo} are in large part eliminated by dividing by G. However, $\dot{\varepsilon}_{os}$ and $\dot{\varepsilon}_{ol}$ reflect a temperature dependence of high-temperature creep of the form:

$$\dot{\varepsilon}_{os} = \dot{\varepsilon}_{oos}\exp\left(-Q/RT\right) \tag{11.3-38}$$

$$\dot{\varepsilon}_{o1} = \dot{\varepsilon}_{ool}\exp\left(-Q/RT\right) \tag{11.3-39}$$

where $\dot{\varepsilon}_{oos}$ and $\dot{\varepsilon}_{ool}$ are constants; Q, R, and T are the creep activation energy, gas constant, and absolute temperature, respectively. The values for the parameters in all of the above equations are:

G = 92.0 – 4.02 10^{-2} T (GPa)

θ_l/G = 3.66·10^{-2}

σ_{so}/G = 2.00·10^{-2} – 9.12·10^{-6} T

σ_{lo}/G = 2.06·10^{-3} + 7.12·10^{-1} T

m = 1/5.35 = 0.187

Q/R = 38533 (K)

$\dot{\varepsilon}_{oos}$ = 1.062·10^{14} (s^{-1})

$\dot{\varepsilon}_{ool}$ = 3.794·10^{12} (s^{-1})

K = 2.0

The combination of the Eq. 11.3-32 and the above strain-rate and temperature laws allow one to generate the complete rate and temperature dependent true-stress/true-strain curves. The yield stress, σ_l, in these equations can be compared to the 0.2% offset yield stress. The ultimate strength, while not specifically denoted in the equations, can be determined by differentiating the Eq. 11.3-32 in accordance with the construction of true stress, σ_u, that corresponds to the engineering ultimate strength:

$$\left.\frac{d\sigma}{d\varepsilon}\right|_{\varepsilon_{pu}} = \theta_l \exp\left(-\varepsilon_{pu}/\varepsilon^*\right) = \sigma_u \tag{11.3-40}$$

where ε_{pu} is the true plastic strain at the ultimate strength which corresponds to the uniform elongation. Solving the above equation and Eq. 11.3-32 simultaneously gives σ_u and ε_{pu}.

11.3.6.2 HT9 Cladding

The deformation behavior of the martensitic-ferritic stainless steel HT9 cladding can be described over a broad range of temperature and strain-rate with the set of equations shown below. These equations are incorporated in FPIN2 and used in calculations of strength and ductility of this alloy at temperatures ranging from room temperature to 1110 K under a variety of loading conditions. The high temperature creep behavior is adequately described by an equation of the Dorn power-law form:

$$\frac{\dot{\varepsilon}_p}{\dot{\varepsilon}_{oos}} = \left(\frac{E}{\sigma_{so}}\right)^n \left(\frac{\sigma_s}{E}\right)^n exo\left(-\frac{Q_c}{kT}\right) \tag{11.3-41}$$

In this equation, $\dot{\varepsilon}_p$ is the steady-state equivalent creep rate normalized by the constant $\dot{\varepsilon}_{oos}$, σ_s is the equivalent applied stress in the creep test normalized by the constant σ_{so}, E is the temperature dependent Young's modulus, Q_c is the creep activation energy, k is Boltzmann's constant, and T is absolute temperature. The temperature dependence of E is expressed as

$$E(T) = 2.12 \cdot 10^{11}\left[1.144 - 4.856 \cdot 10^{-4} T\right] \quad (Pa) \tag{11.3-42}$$

and the remaining parameters in the creep equation are given by

$$\dot{\varepsilon}_{oos} = 5.1966 \cdot 10^{10} \ \left(s^{-1}\right)$$

$$\sigma_{so}/E = 3.956 \cdot 10^{-3}$$

$$n = 2.263$$

$$Q_c/k = 36739 \ (K)$$

The flow-stress/strain-hardening behavior can be described by an equation of the type

$$\frac{\sigma_e}{E} = \frac{\sigma_s}{E} - \frac{\sigma_s - \sigma_l}{E} \exp\left(-\frac{\bar{\varepsilon}_p}{\varepsilon^*}\right) \tag{11.3-43}$$

where σ_e is the equivalent flow stress at some value of true equivalent plastic strain $\bar{\varepsilon}^p$ (defined in Eq. 11.2-26), measured from the reference state of as-heat-treated material $\left(\bar{\varepsilon}^p = 0\right)$. As described in Section 11.3.6.1, θ_l is the yield stress of as-heat-treated material, ε^* is a temperature dependent parameter extracted from the hardening rate at the ultimate strength, and σ_s is the saturation stress, or steady-state flow stress, approached at a large plastic strain and assumed compatible with the stress in the above steady-state creep equation. It has been found that assuming that the yield stress $\sigma_l = 0.8\sigma_s$ throughout allows the generation of flow stress-strain curves that agree well with data. The true stress at the ultimate strength (maximum load), after differentiating Eq. 11.3-43, is given by

$$\frac{\sigma_u}{E} = \frac{\sigma_s - \sigma_l}{E\,\varepsilon^*} \exp\left(\frac{-\varepsilon_{pu}}{\varepsilon^*}\right) \tag{11.3-44}$$

where ε_{pu} is the true strain at the ultimate strength corresponding to the uniform elongation. Simultaneously solving this equation in conjunction with the flow stress equation evaluated at ε_{pu}, the following expression is obtained for the quantity ε^*:

$$\varepsilon^*(T) = 0.12733 - 3.5027 \cdot 10^{-4} T + 2.9934 \cdot 10^{-7} T^2 \tag{11.3-45}$$

An equation to model the transition between high-rate, low-temperature, rate independent flow behavior and creep behavior has the form

$$\frac{\sigma_s}{E} = \frac{\sigma_{so}}{E}\left\{1 - \exp\left[\left(\frac{\bar{\varepsilon}_p \exp\left(Q_c / kT\right)}{\varepsilon_{oos}}\right)^{K/n}\right]\right\}^{1/K} \tag{11.3-46}$$

Because of microstructural changes that occur during long-time creep testing of HT9, and the effects they have on flow stress, there is not a smooth transition between short term tensile behavior and creep behavior. However, setting the non-physical fitting parameter as $K = 0.2$, and with all the other parameters set as indicated above, Eq. 11.3-46 follows the tensile data quite well, and reduces to the power-law creep equation at very low strain rates.

For temperatures above the completion of the γ transformation temperature (1233 K), the flow stress model in FPIN2 assumes that the deformation rate for HT9 cladding is the same as that given by the Type 316 SS and D9 cladding equations in Section 11.3.6.1. A simple mixture rule is used to calculate the deformation rates in the α-γ transition region (1110K-1233K).

11.3.7 Fuel-Cladding Eutectic Formation

An additional complication for metallic fuels is the formation of a low melting point eutectic alloy between the fuel and the cladding that can contribute to fuel element failure during transient overheating events. The eutectic alloy forms due to interdiffusion of fuel and cladding constituents at the fuel-cladding interface. It melts at a temperature lower than the fuel and cladding solidus temperatures.

11.3.7.1 Eutectic Penetration of the Cladding

The primary effect of the liquid eutectic alloy formation on fuel element failure is thinning of the cladding wall. The liquid does not further damage the remaining cladding tendon by mechanisms such as liquid metal embrittlement. Experimental data documenting this effect comes from constant temperature time-to-failure experiments on irradiated EBR-II fuel elements and form out-of-pile dipping tests of penetration of iron by molten uranium-iron eutectic alloy. These data have recently been reviewed and the following correlation has been recommended [11-15]

$$\dot{M} = \begin{cases} 0 & T < 1353K \\ 922 + 2.93(T-1388) - 0.215(T-1388)^2 + 0.001134(T-1388)^3 & 1355K \le T \le 1506K \\ \exp\left(22.85 - \dfrac{27624}{T}\right) & T > 1506\,K \end{cases} \tag{11.3-47}$$

where $\dot{M}$ is the melt rate in $\mu m/s$, and T is the absolute temperature in Kelvins. The major feature of the data and these equations is that the melt rate is very rapid for temperatures above 1353 K. For typical cladding dimensions, this means that cladding will completely melt-through is somewhat less than one second once molten fuel reaches 1353K. On the other hand, for the transient rate of concern for a typical FPIN2 application, negligible cladding melt-through occurs until this "rapid eutectic attack" temperature is reached.[6] The Eq. 11.3-47 is used in cladding failure criterion subroutine of FPIN2 to calculate wall thinning.

11.3.7.2 Eutectic Release of Cladding Axial Restraint

When fuel and cladding are in contact, FPIN2 has an option that allows that fuel and cladding to either slip freely axially or to be locked together. In the latter option, it is assumed that the fuel and cladding remain locked, either by metallurgical bonding or by friction, at temperatures below the assumed eutectic alloy melting threshold, T_{th} (an input in the code). At temperatures above T_{th}, the fuel and cladding are assumed to slip freely because of the liquid phase that forms at the fuel cladding interface. This discontinuity in the cladding axial constraint model of FPIN2 at the assumed eutectic alloy melting temperature causes a sudden drop in stress in both fuel and cladding

[6] The rate at 1000K is about 10^{-2} μm/s, which would require 10 hours to completely penetrate the full cladding wall thickness.

elements as the fuel expands slightly in the axial direction and contracts in the radial direction due to elastic recovery.

When the fuel-cladding gap is open, the fuel and cladding axial displacements are calculated independently. When the fuel and cladding are locked together, the increments in axial strain in the fuel are assumed to be equal to the increments in axial strain in the cladding. This is handled in mechanics calculation by modifying the terms in the stiffness matrix. Specifically, the finite-element algorithm is solved for the resultant fuel and cladding axial forces by combining the fuel and cladding stiffness matrices in a non-iterative procedure. In this procedure, the two equations for the axial displacements are replaced by a single equation for their joint displacement. The redundant equation is then replaced with an identity so that the size of the stiffness matrix and all the associated coding remains the same. When the sudden release of cladding restraint occurs at eutectic alloy melting point, fairly large changes take place in the axial displacements. However, experience has shown that, due to the robust procedure used, this substantial sudden change in the mechanics causes no computational difficulties.

11.3.8 Fuel Element Failure

The failure of the cladding due to temperature and pressure transients is essentially independent of fuel type except that failure in metal fueled elements is augmented by eutectic formation which penetrates and, in effect, thins the cladding as discussed in the previous section. Also, the loss in cladding stiffness is not considered in calculating the continued deformation of the cladding in the oxide fuel version of FPIN2. For conditions where simultaneous eutectic erosion and plastic deformation are important, oxide fuel version under-predicts the permanent cladding strains at the time of failure. Therefore, the FPIN2 analysis of cladding deformation has been modified to account for this eutectic thinning and to determine the permanent cladding strain remaining after a transient more accurately.

The technique that has been implemented in the FPIN2 cladding deformation model to account for the eutectic attack uses an effective ligament thickness ratio to decease the contribution that the material stresses in a given element make to the overall balance between internal and external forces. Elements that are fully liquid are assumed to have a ligament thickness ratio of zero and those that are solid are assumed to have ligament ratio of one. An element that has partially liquefied then has a ratio equal to the fraction of the element that is still solid. In other words, the effect of eutectic formation is included in FPIN2 by considering only the thickness of unaffected cladding that is available to carry the load. This model has the additional benefit that it can easily be modified to account for other damage mechanisms such as cavitation and void growth during tertiary creep. In the current version of the FPIN2, however, these additional mechanisms are not considered.

For transients with relatively short time scale, the eutectic penetration is a factor only if the cladding temperature exceeds the “rapid eutectic attack” temperature (1353K) where the penetration rate increases by three orders of magnitude. The change in cladding wall thickness above 1353K is calculated using Eq. 11.3-47 for Type

316 SS, D9, and HT9 cladding. At temperatures below 1353K, the rate of eutectic penetration is generally insignificant and assumed to be zero.

Cladding rupture is predicted in the code by using the life fraction criteria. The TCD-2 life fraction criterion [11-16] is used for the fuel elements with D9 and Type 316 stainless steel cladding; and the HEDL transient Dorn parameter correlation [11-17] is used for the fuel elements with HT9-cladding. The fuel adjacency effect in the TDC-2 correlation has been neglected. The life fraction over a time step, *dt*, is calculated from the rupture time, t_r, for the instantaneous average cladding temperature, T_c, and hoop stress, σ_c. Life fractions are summed in the usual way so that cladding failure is predicted to occur at time t_f when

$$\int_0^{t_f} \frac{1}{t_r(\sigma_c, T_c)} dt = 1 \tag{11.3-48}$$

The location of the failure is the location of first axial cladding segment to reach a life fraction of 1.0. The hoop stress in the cladding tendon is calculated by the thin-shell equations consistent with the methodology used in developing the life fraction correlations. The thickness of this tendon is reduced by the amount of eutectic attack.

11.4 Integration of FPIN2 into SASSYS/SAS4A and Usage of Integrated Model

A general purpose SAS-FPIN2 interface has been designed and most of the communication between the two codes is established at this interface minimizing the impacts of coupling on both codes. This coupling strategy allows for maintaining the stand-alone capability of the two codes while assuring that any future improvements to FPIN2 are automatically reflected in SASSYS/SAS4A.

11.4.1 SAS-FPIN2 Coupling Methodology

Two modes of SAS-FPIN2 coupled operations are provided. In the stand-alone mode, FPIN2 reads its own input deck and executes without linking to SASSYS/SAS4A. This mode is provided primarily for verification/debugging purposes, to allow independent development of FPIN2, and to allow it to continue its role as a tool for thermo-mechanical analysis of individual fuel pins.

In the interfaced mode, FPIN2 replaces the SASSYS/SAS4A metal fuel element mechanics module DEFORM-5 and calculates the updated dimensions, stresses, and strains at the end of each time step. These FPIN2 results are then made available for use in the analysis of accident energetics by providing estimates of axial expansion of fuel, time and location of cladding failure, and the condition of the fuel element at the time of the failure (although the communication between FPIN2 and the SAS4A in-pin and ex-pin fuel relocation modules, PINACLE and LEVITATE, is not yet established). In the interfaced mode, some of the input necessary to run FPIN2 is included in the SASSYS/SAS4A input deck, and the remaining is interpreted from corresponding SASSYS/SAS4A variables.

11.4.1.1 Stand-alone FPIN2 Calculation

In the stand-alone mode, FPIN2 is run by a call to main FPIN2 driver routine, FPMAIN. In this mode, FPIN2 performs complete thermal-mechanical calculations for a single fuel element. When the heat transfer option to calculate the coolant and structure temperatures is invoked, the fuel element is assumed to be surrounded by a circular coolant channel and an outer wall in pin-in-a-pipe geometry. The code also provides an option in which the cladding outer surface temperature may be specified as a function of time to drop the coolant channel and structure calculations. This mode is mainly provided for direct verification and code debugging purposes.

In the stand-alone mode, FPIN2 input is appended at the end of SASSYS/SAS4A input deck after the ENDJOB record. The stand-alone FPIN2 input deck consists of the following records entered in free format:

1. Title,
2. Integer data (including integer debug data),
3. -1/ End of Integers,
4. Decimal data (including decimal debug data),
5. -1/ End of Decimals.

Integer and decimal input data are entered in a form similar to the SASSYS/SAS4A input data. Each of the FPIN2 input variables has an assigned location number. The first entry in a line of input data is the location number of the first member of the set of input data values. The second entry is the number of data values that follow. Integer and decimal input data fields are initialized to zero before reading in the data; therefore, a variable does not have to be read in if it has the value of zero. A line of data may continue over several records; however, the maximum number of data values in a line is limited with 2000. The primary unit system for stand-alone FPIN2 input and output is CGS with exception of pressure which is specified in Bar. Temperature is specified in Kelvin. The full list of FPIN2 input variable for stand-alone calculation along with a brief description for each variable is provided in Appendix 11.2.

11.4.1.2 Interfaced SAS-FPIN2 Calculation

The SAS-FPIN2 interface consists mainly of the steady-state and transient FPIN2 driver routines. The steady-state driver, FPINIT, performs setup of FPIN2 for the interfaced calculation and initializes FPIN2 input from SASSYS/SAS4A data. This routine is executed only once prior to the transient calculations. The transient FPIN2 driver routine, FPDRIV, incorporates the time-advancement scheme and interfaces dynamic variables between the two codes.

During the initialization of FPIN2 from SASSYS/SAS4A input, interface routine FPINIT looks for inconsistencies in fuel element modeling, prints diagnostic messages, and terminates the execution if necessary. The main inconsistencies that a user should be aware of are summarized below:

1. A gas plenum below the fuel column is not allowed in FPIN2; therefore, the execution is terminated if SASSYS/SAS4A input variable IPLUP (Block 1, location 5) is non-zero.
2. If the fuel element contains axial blankets, i.e., MZUB and/or MZLB (Block 51, location 27 and 28, respectively) are non-zero, a warning message is printed since FPIN2 mechanics calculation is not normally performed for the axial segments containing blanket fuel.[7]
3. An error message is printed and execution is terminated if the number of axial segments in fuel exceeds FPIN2's limit (20),
4. An error message is printed if SASSYS/SAS4A input variable IPOWRZ (Block 51, location 364) is non-zero (applicable only when IHTFLG≠0 (Block 51, location 287)).
5. Cross-checking of the input data for abnormalities are also performed (such as zero pin pressure) and diagnostic messages are printed.

Since FPIN2 has been primarily developed for the transient analysis of fuel elements, it lacks models to describe pre-transient irradiation features such as fuel restructuring, fission gas retention and fuel-cladding gap narrowing. These pre-transient conditions are to be provided as input for the metallic fuels as discussed in Section 11.4.3. The as-irradiated geometry, fuel elongation, fission product and porosity distributions, and the effect of fast neutron fluence on cladding are typically obtained from the relevant in-reactor fuel performance database at a desired burnup, or from steady-state fuel performance codes such as LIFE-METAL [11-18] and STARS [11-6]. FPIN2 has the capability to interpret its input from the LIFE-METAL output. This capability is also extended to the integrated SAS-FPIN2 model.

Normally, FPIN2 heat transfer is by-passed in the interfaced mode and the fuel element temperatures are lined with SASSY/SAS4A calculated fuel, cladding, plenum, and cavity temperatures. To accomplish this by-pass, the FPIN2 mechanics/thermal-hydraulics boundary is identified, and routines that are used in heat transfer calculation are isolated. All the common block variables that are used in the mechanics calculation (but altered in one of these heat-transfer routines) are linked with their SASSYS/SAS4A counterparts. The FPIN2 results for stresses and displacements are in turn made available to SAS4A for the estimates of axial expansion of fuel and associated reactivity effects, time and location of cladding failure, and the condition of the fuel at the time of failure.

In the interfaced mode, setting the input flag, IHTFLG, may also turn on FPIN2's own heat transfer model. The option for including FPIN2 heat transfer model is mainly provided for debugging and code verification purposes. It requires additional data to be interfaced regarding fuel pin heat generation rate and cladding outer surface temperature for each axial segment at each time step as the dynamic boundary

[7] FPIN2 mechanical analysis can be performed for axial blankets by describing them as a type of fuel with known material mechanical properties.

condition. When this option is set, FPIN2 uses its own built-in metallic fuel thermal property routines.

In order to establish consistency between SASSYS/SAS4A and FPIN2 calculations in the interfaced mode, some modifications to the FPIN2 code were necessary. Major changes to FPIN2 for this integration are summarized below:

1. Generic precision conversions are performed by combining all type declaration statements in a file and replacing them in each subprogram with an INCLUDE statement referencing this file.
2. Along the same line, type specific intrinsic functions are converted to their generic equivalents.
3. Various table interpolations for time-dependent boundary conditions (pin power and cladding outer surface temperature when IHTFLG=1) are bypassed and these variables are linked with their SASSYS/SAS4A calculated counterparts.
4. Various calls to built-in FPIN2 material thermal property subprograms are also bypassed and the thermal properties that are needed in FPIN2 mechanics calculation are substituted with their SASSYS/SAS4A calculated equivalents.
5. Steady-state and transient pin plenum gas temperature is interfaced with the corresponding SASSYS/SAS4A variable.
6. Constant liquid eutectic alloy melting temperature is converted to a variable and listed as an integrated SAS-FPIN2 model input, XEUTHR.
7. Initial cladding effective inner surface wastage is described as a new integrated SAS-FPIN2 model input variable and incorporated into FPIN2 by defining it as part of the variable for cladding wall thinning due to eutectic penetration.
8. The constant coolant channel pressure is converted to a dynamic array variable and interfaced with its axially varying time-dependent SASSYS/SAS4A counterpart.

All these changes are implemented in such a way that they do not affect the stand-alone performance of FPIN2.

The radial mesh structure for SASSYS/SAS4A, stand-alone FPIN2, and interface SAS-FPIN2 calculations are shown in Fig. 11.4-1. As presented in Chapter 3, the radial mesh structure in SASSYS/SAS4A for fuel elements at a given axial segment can be set up based on either equal radial difference or equal mass principle. In either case, the boundary nodes are the half sixe as shown in Fig. 11.4-1b. In FPIN2, on the other hand, finite elements are initially defined in a mesh based on an equal radial difference principle with all elements having the same thickness as shown in Fig. 11.4-1a. In order to avoid extensive remapping of the thermal and mechanical variables between two meshes during the interfaced calculations, the consistency between the initial mesh structures is accomplished by pulling SASSYS/SAS4A-calculated mesh information into

FPIN2 common blocks, and forcing FPIN2 to use the same mesh structure in the fuel and cladding (Fig. 11.4-1c). When FPIN2 heat transfer is by-passed, however, this procedure requires substitution of mesh-centered temperatures for boundary nodes, namely T_{f1}, T_{fNDRF}, T_{c1}, and T_{c3} (locations marked with a "*" in Fig. 11.4-1c), that are not calculated in SASSYS/SAS4A. In the interfaced mode, these temperatures are approximated with a linear interpolation between the temperatures of the neighboring nodes.

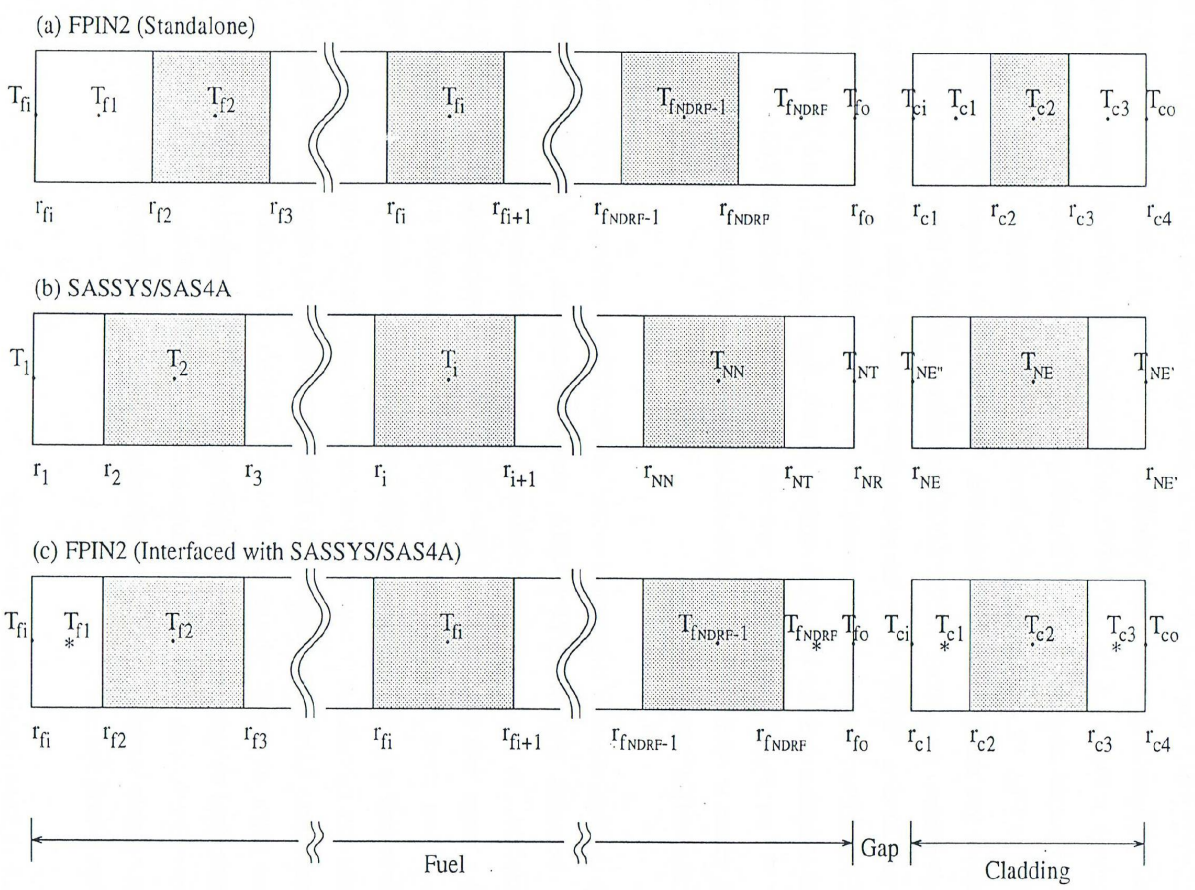

Fig. 11.4-1: Radial Mesh Structure and Temperature for an Axial Segment in (a) FPIN2 Code, (b) SASSYS/SAS4A, and (c) Integrated SAS-FPIN2 Model.

Although the fuel element mechanics model of FPIN2 uses an implicit solution scheme, the interaction between the SASSYS/SAS4A thermal-hydraulics and FPIN2 mechanics calculations is explicit. In the SASSYS/SAS4A code system, a multi-level time-step hierarchy is used in which a main time step is divided into one or more primary-loop, heat transfer, and coolant dynamics time steps as described in Chapter 2. The control over the length of a computational time step is performed using a variety of internal and user-specified restrictions. The FPIN2 mechanics calculation is performed at the each heat transfer time step using newly calculated temperatures. Limitations imposed by stability and accuracy requirements assure that heat-transfer time steps are small enough to avoid the problem of unstable results between the thermal and mechanical calculations due to explicit coupling. The implicit treatment in FPIN2 is somewhat inconsistent with the explicit nature of the SASSYS/SAS4A code system and it often results in a notable increase in computation time. However, the capabilities gained by this coupling are often well worth this additional computational cost.

11.4.1.3 Subroutine Descriptions and Flow-charts

The list of SAS-FPIN2 interface routines is presented in Table 11.4-1. In the stand-alone mode, the FPIN2 main program is called form the SASSYS/SAS4A steady-state driver routine SSTHRM and FPIN2 is executed without interfacing to SASSYS/SAS4A. In the interfaced mode, FPIN2 is coupled to the rest of the SASSYS/SAS4A calculations through two main driver subroutines, FPINIT and FPDRIV. First the steady-state FPIN2 driver routine FPINIT is called from SSTHRM for initialization of FPIN2 for interfaced calculations. A flowchart for the FPINIT subroutine is shown in Fig. 11.4-2. Then, during the transient calculations, SASSYS-SAS4A thermal-hydraulic manager TSTHRM calls for the transient interface routine FPDRIV that acts as the FPIN2 transient driver.

Table 11.4-1: SAS-FPIN2 Interface Subroutines

Subroutine Name	Description
FPMAIN	In the stand-alone mode, FPIN2 driver (main program)
FPINIT	In the interfaced mode, steady-state FPIN2 initialization routine
FPDRIV	In the interfaced mode, FPIN2 transient driver routine
SASTMP	In the interfaced mode, SAS-FPIN2 thermal-hydraulics interface (when FPIN2 heat transfer module is by-passed)
FPNOUT	In the interfaced mode, output of the FPIN2 results

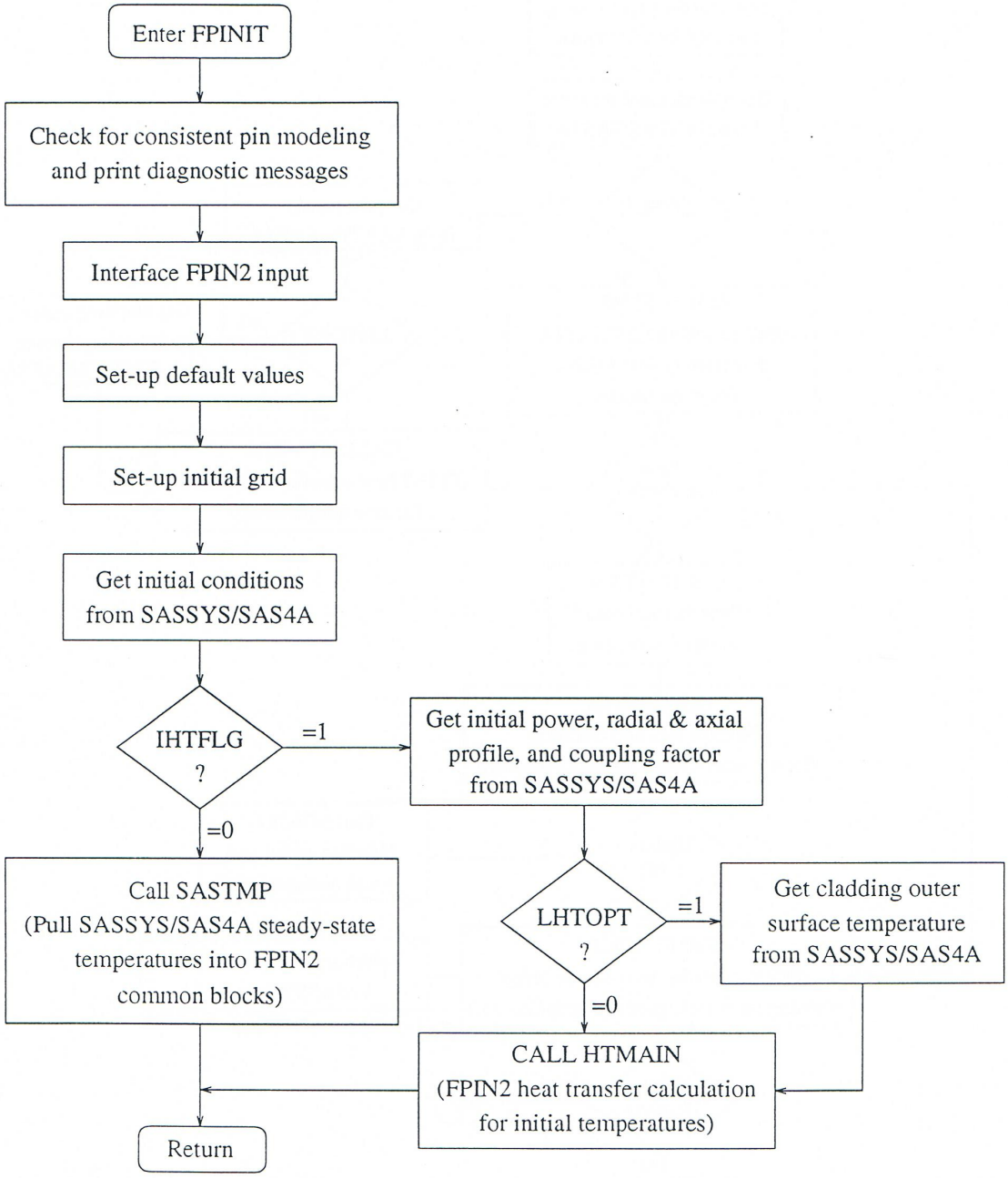

Fig. 11.4-2: FPINIT Subroutine Flow Diagram

Subroutine FPDRIV basically includes the section of FPMAIN that is used for the time advancement scheme. This time advancement scheme is preceded by an upper interface routine, SASTMP that pulls SASSYS/SAS4A calculated temperatures into FPIN2 common blocks, and is followed by a lower interface section that takes FPIN2 updated axial and radial mesh information and puts it back into SASSYS/SAS4A common locations. SASTMP is also used by steady-state interface routine FPINIT to extract the initial temperature distribution from SASSYS/SAS4A. A flowchart for the subroutine FPDRIV is presented in Fig. 11.4-3.

11.4.2 Input Description for Interfaced SAS-FPIN2 Calculation

Two groups of input variables are identified for interfaced SAS-FPIN2 calculations. Integrated model variables that describe the mode of the interfaced calculation and FPIN2 variables that are not readily provided by SASSYS/SAS4A are included in SASSYS/SAS4A common blocks INPCHN (for integer variables) and PMATCH (for real variables). The list of these "new" variables is provided in Table 11.4-2.

Another category includes input variables that are provided by SASSYS/SAS4A calculations and/or are translated from SASSYS/SAS4A input. The list of these variables along with SASSYS/SAS4A counterparts is presented in Table 11.4-3. The variables in Table 11.4-2 and Table 11.4-3 constitute the full list of input parameters necessary to run FPIN2 in the interfaced mode. Further information on some of the input parameters related to pre-transient fuel element characterization is given in the following section. When interpreting FPIN2 input from SASSYS/SAS4A data, dimensional conversions are necessary since the principal unit systems for SASSYS/SAS4A and FPIN2 and SI and CGS, respectively.

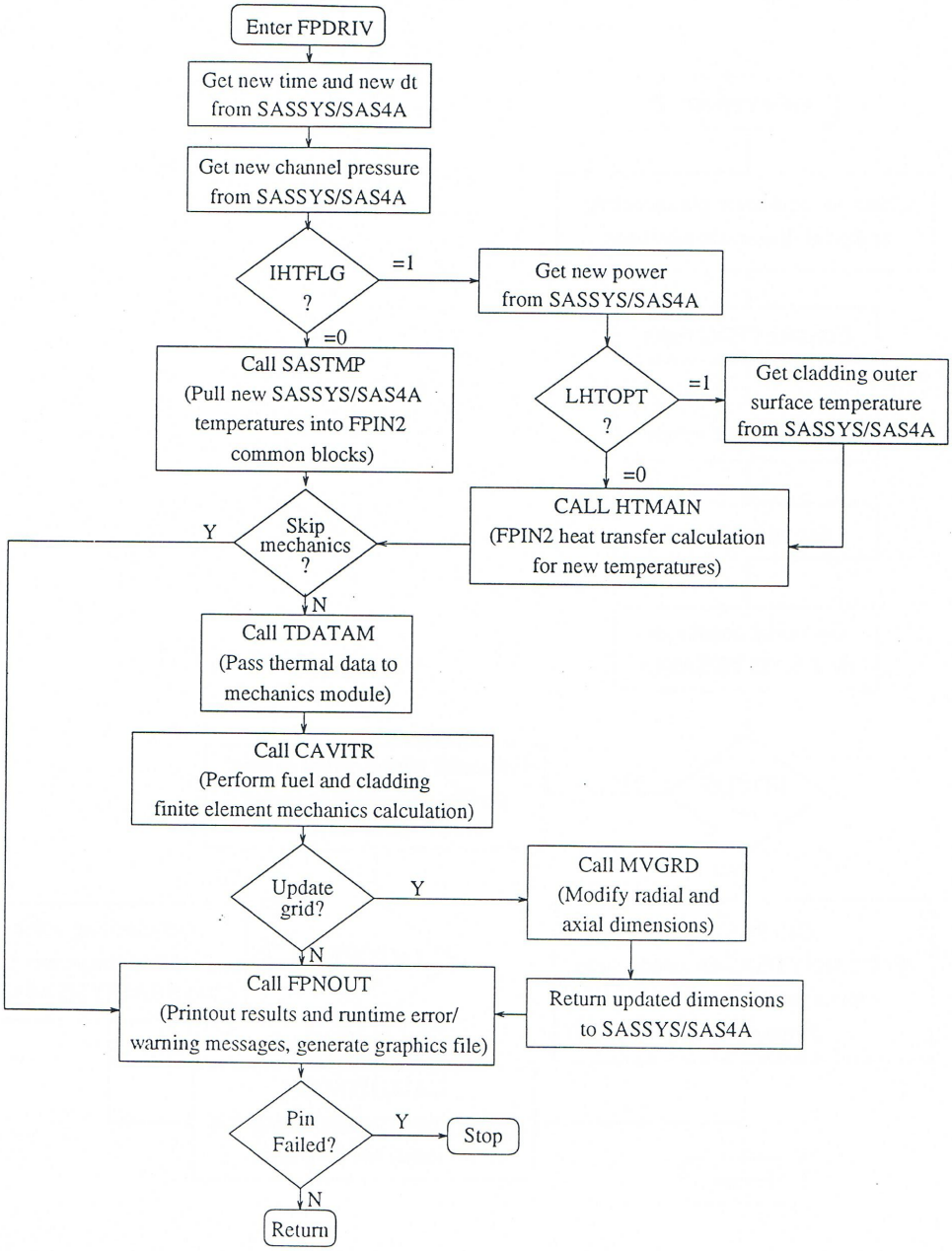

Fig. 11.4-3: FPDRIV Subroutine Flow Diagram

Table 11.4-2: Input Variables for Integrated SAS-FPIN2 Model

BLOCK 51 * INPCHN

Location	Symbol	Value	Definition/Comments
285	IFPIN2	=0	Do not use FPIN2 metal fuel model
		=1	Use FPIN2
	(Note: No other data required when IFPIN2=0)		
286	IFPI01	=0	Use FPIN2 in interfaced mode
		=1	Use FPIN2 in standalone mode
	(Note: No other data required when IFPI01=1)		
287	IHTFLG	=0	Bypass FPIN2 heat transfer calculation
		=1	Include FPIN2 heat transfer calculation
288	LHTOPT	=0	Perform heat transfer calculation including coolant and wall
		=1	Perform heat transfer calculation with input value of cladding outer surface temperatures
289	LCRACK	=0	No fuel cracking
		=1	Radial fuel cracks included
290	LFPLAS	=0	Allow creep-plastic strains in fuel
		=1	Suppress creep-plastic strains in fuel
291	LCPLAS	=0	Allow creep-plastic strains in clad
		=1	Suppress creep-plastic strains in clad
292	LFSWEL	=0	Allow swelling-hotpressing strains in fuel
		=1	Suppress swelling-hotpressing strains in fuel
293	LCSWEL	=0	Allow swelling strains in clad
		=1	Suppress swelling strains in clad
294	LLRGST	=0	Large strain analysis
		=1	Small perturbation analysis
295	LFCSLP	=0	Fuel-clad locked when gap is closed
		=1	Independent fuel-clad axial displacement
296	LOUTSW	=0	No detailed printing of results – summary only
		=1	Normal detailed printout under LFREQA, MFREQA, and LFREQB control
297	LFREQA		Initial print frequency, number of time steps between normal detailed printout
298	MFREQA		Total number of time steps under LFREQA control

BLOCK 51 * INPCHN

Location	Symbol	Value	Definition/Comments
299	LFREQB		Final print frequency
300	LGRAPH	=0	Do not write graphics file
		=1	Write a graphics data file
301	LDBOUT	=0	Do debug output
		=1	Add debug output to regular LOUTSW=2 output
302	LDBSTP	=0	Program stops when molten cavity freezes
		=1	Ignore this program stop
303	LDBFPL	=0	Use recommended fuel flow stress (Eq. 11.3-16)
		=1	Use simple power law fuel creep: $\dot{\varepsilon} = C_0 \sigma_e^{C_1}$ (Note: XFPLC0 and XFPLC1 are required)
304	LDBFDV	=0	Use recommended fuel swelling-hotpressing (Eq. 11.3-30)
		=1	Use equilibrium swelling model (ANL-IFR-6 and -23)
		=2	Use simple power law fuel swelling: $\dot{\varepsilon} = C_0 \sigma_m^{C_1}$ (Note: XFDVC0 and XFDVC1 are required)
305	LDBCPL	=0	Use recommended clad flow stress
		=1	Ideal plastic flow for clad: $\sigma_y = C_0 + C_1 \bar{\varepsilon}^p$ (Note: XCIPL0 and XCIPL1 are required)
		=2	Use high-temperature power-law creep
		=3	Use simple power law clad creep: $\dot{\varepsilon} = C_0 \sigma_e^{C_1}$ (Note: XCIPL0 and XCIPL1 are required)
306	LGPRES		(Not currently used)
307	LGAPCL	=0	Use fuel-clad opening/closure model
		=1	Fuel-clad gap always closed
308	LCPROP	=0	Use material property correlations (when IHTFLG=1)
		=1	Use temperature independent material properties (when IHTFLG=1)
309	LSKIPM	=0	Perform mechanical calculations
		=1	Bypass mechanical calculations, heat transfer only (when IHTFLG=1)
310	LGCLOS	=0	Use gap closure routine at 100% fuel melting

BLOCK 51 * INPCHN

Location	Symbol	Value	Definition/Comments
		=1	Do not close gap (if open) at 100% fuel melting
311-334	LDBOTA(J)		Axial debug print vector (0=no-print, 1=print)
355-345	LDBOTF(I)		Fuel radial debug print vector (0=no-print, 1=print)
346-348	LDBOTC (IC)		Clad radial debug print vector (0=no-print, 1=print)

BLOCK 63 * PMATCH

Location	Symbol	Definition/Comments
105	XEUTHR	Liquid eutectic threshold temperature (K) (Default=988.) (See FSPEC in Block 65, location 1 for consistent input)
106	XGBFRA	(Not currently used)
107-130	XCLDHR(J)	Pre-transient hardness parameter used in clad flow stress calculation. (Default value is 0.223, the value appropriate for 20% CW unirradiated stainless steel.)
131	XFPLC0	Fuel power law creep constant C_0 (when LDBFPL=1)
132	XFDVC1	Fuel power law creep constant C_1 (when LDBFPL=1)
133	XFDVC0	Fuel power law swelling constant C_0 (when LDBFDV=2)
134	XFDVC1	Fuel power law swelling constant C_1 (when LDBFDV=2)
135	XCIPL0	Clad idealized flow stress constant C_0 (when LDBCPL=1 or 3)
136	XCIPL1	Clad idealized flow stress constant C_0 (when LDBCPL=1 or 3)
137	XHTERR	Relative convergence criterion for heat transfer calculation (when IHTFLG=1) (Default=0.0005)
138	XEPSCA	Relative convergence criterion for cavity pressure (Default=0.001)
139	XEPSFE	Relative convergence criterion for finite element analysis (Default=0.0005)
140	XEPTES	Relative convergence criterion for plastic-creep strains (Default=0.0005)
141	XEVTES	Relative convergence criterion for swelling strains (Default=0.0005)

Table 11.4-3: FPIN2 Input Variables that are Provided by SASSYS/SAS4A Calculations and/or Interpreted from SASSYS/SAS4A Input.

Description	**FPIN2 Variable**	**SASSYS/SAS4A Counterpart**
Metal fuel type (U-Fs, binary, or ternary)	IFTYPE	IMETAL
Cladding type (Type 316, D9, or HT9)	ICTYPE	ICTYPE
Number of axial segments in fuel column	NDZ	MZ
Number of radial elements in fuel	NDRF	NT
Number of radial elements in cladding	NDRC	3
Transient initiation time (s)	TZERO	0.
Computation time step size (s)	DTIME	DTP
Initial height of axial segments	DZ(J)	AXHI(J)
Initial length of plenum (cm)	ZPLENM	PLENL
Initial length of bond sodium in plenum (cm)	ZPLNA	BONDNA, pin geometry
Gas constant for plenum gases (Bar-cm^3/gm-K)	PLGASR	RGASSI, HEMM, FGMM, P0GAS, FGFI
Gas constant for central cavity gases (Bar-cm^3/gm-K)	GASCON	RGASSI, HEMM, FGMM
Initial pin pressure (Bar)	PINT	P0GAS
Reference temperature at which PINT is specified (K)	PLTREF	TR
External (channel) pressure (Bar)	PEXT	PCOOL2(J)
Plenum gas temperature (K)	PGASTM	TGASP2
Description	FPIN2 Variable	SASSYS/SAS4A Counterpart
Peak fuel burnup (at.%)	BURNUP	BURNFU
Fuel radial mesh array (cm)	RADF(I,J)	R(I,J)
Clad radial mesh array (cm)	RADC(I,J)	R(NE,J), R(NEP,J)
Distribution of fission gas in closed porosity or in solution (gm/cm^3)	FISGAS(I,J)	ROGSPI, BURNFU, FIFNGB
Fraction of FISGAS on grain boundaries (Default=0.10)	GBFRAC	FIFNGB
Distribution of total fuel porosity	PORES(I,J)	PRSTY2(I,J) (based on PRSTY(IFUELV))

Description	FPIN2 Variable	SASSYS/SAS4A Counterpart
Axial profile of cladding fluence (10^{22} n/cm^2)	CLDFLU(J)	BURNFU, FPDAYS, PBAR(J), FLTPOW, AXHI(J)
Effective cladding inner surface wastage thickness (cm)	WASTE	TWASTI, TWASTO
Mass of fuel elements (gm)	FMASS(I,J)	FUELMS(I,J)
Mass of cladding elements (gm)	CMASS(I,J)	DENSS, cladding geometry.
Distribution of Pu in ternary fuel	FRACPU(I,J)	FUPUMS(I,J), FUELMS(I,J) (based on PUZRTP(IFUELV))
Distribution of Zr in ternary fuel	FRACZR(I,J)	FUZRMS(I,J), FUELMS(I,J) (based on PUZRTP(IFUELV))
Fuel solidus temperature (node-by-node) (K)	FTSOL(I,J)	TSOLIJ(I,J)
Fuel liquidus temperature (node-by-node) (K)	FTLIQ(I,J)	TLIQIJ(I,J)
Normalized time dependent reactor power (when IHTFLG=1)	POWNEW	QMULT
Pin power coupling factor (when IHTFLG=1)	QCONST	1.
Axial profile of energy generation rate (normalized) (when IHTFLG=1)	QAX(J)	PSHAPE(J)
Radial profile of energy generation rate (W/gm) (when IHTFLG=1)	QR(I,J)	RADPRS(I,J), POW, GAMTNE, GAMTNC, GAMSS, FUELMS
Cladding outer surface temperature (K) (when IHTFLG=1 and IHTOPT=1)	TCSURF(J)	T2(NEP,J)

11.4.3 Pre-transient Fuel Element Characterization

The steady-state fuel element characterization forms the initial conditions from which the transient calculations begin. The FPIN2 mechanics calculation is initiated from a stress-free state for hot and irradiated (swollen) fuel elements. Prior irradiation of fast reactor fuel elements influences their thermal and mechanical response during accident transients significantly. The pre-transient features that are more important for metallic fuels are fuel geometry, fission product, alloy, and porosity distributions, fuel elongation, and the effects of fast neutron fluence on transient cladding properties. These initial conditions can be obtained from the in-reactor fuel performance database or from a fuel performance computer code. In this section, the methods that are suggested to determine the fuel element pre-transient characterization are outlined.

11.4.3.1 Zone Formation

Post-irradiation destructive examinations of ternary fuel pins irradiated in EBR-II reveal significant migration of plutonium and zirconium. This redistribution produces distinct zones that are associated with different metallurgical phases. Micrographs from irradiated ternary fuel pins typically show a three-ring structure that could be separated physically for examination [11-19]. Analysis of these rings reveals that the intermediate zone is depleted in zirconium while the inner and outer zones are enriched in zirconium. The weight fraction of plutonium, on the other hand, remains nearly uniform. The Zr deficient central zone generally consist of the high temperature γ phase in which all constituents are mutually soluble in the solid sate as described in Section 11.3.4. The primary influence of alloy redistribution and zone formation on transient fuel response is through the changes in fuel material properties with alloy content. The most dramatic change is in the fuel solidus temperature where zirconium depletion may lead to initial fuel melting at a radial location other than the hotter axial centerline.

SASSYS/SAS4A provides capabilities to model this fuel composition variation by zone in metallic fuels (IMETAL=2 in Block 51, location 189) as discussed in Section 10.3.5. This multiple radial fuel zone option is invoked by setting IFUELC=1 (Block 51, location 193). The distributions are determined by fixing the zone boundaries and the alloy content of the each zone (see input variables IZNC (Block 51, location 366-389), IZNM (Block 51, location 390-413), and MFTZN (Block 51, location 414-485)). The representative alloy distributions that are chosen to characterize ternary fuel to be analyzed are specified in the input as weight fractions for each fuel type (PUZRTP in Block 13, location 1300-1315). These distributions are used in the fuel material property routines to determine variations in properties with alloy content.

SASSYS/SAS4A converts this zone information to internal arrays that describe metal fuel composition and composition-dependent quantities on a node-by-node basis. In the integrated SAS-FPIN2 model, FPIN2 interfaces with these internal SASSYS/SAS4A arrays to initialize variable FRACPU(I,J), FRACZR(I,J), FTSOL(I,J), FTLIQ(I,J) and FMASS(I,J).

11.4.3.2 Fission Gas Distribution

Fission gas plays an important role in transient fuel element response. The gas that is retained in the fuel during steady-state irradiation provides a source for expansion of both solid and liquid fuel during overheating. The quantity of fission gas in the plenum is also important since the plenum pressure is a major contributor to cladding loading. The distribution of fission gas retained in the fuel matrix is specified as input in FPIN2 (FISGAS(I,J)). Part of this gas is assigned to grain boundary bubbles (GBFRAC) and the remainder of the gas is assumed to be in solution or in small bubbles within the fuel grains. A number of models that address the various aspects of fission gas behavior are available. One of these, the STARS code gives a detailed self-consistent picture of the distribution of the gas between the fuel matrix, grain boundaries, edge tunnels, large pores, and the plenum [11-6].

The fraction of the retained gas on the grain boundaries increases with burnup as more gas is released and as the plenum pressure becomes significant compared to surface tension constraint on the grain boundary bubbles. In the integrated model, the distribution of fission gas in fuel closed porosity and in solution is calculated from SASSYS/SAS4A input variables according to following formula

$$\mathrm{FISGAS(I,J)} = \mathrm{ROGSPI}\cdot \mathrm{BURNFU}\cdot(1-\mathrm{FIFNGB})\cdot 1\cdot 10^{-3} \tag{11.4-1}$$

where the fraction of fission gas on grain boundaries is simply

$$\mathrm{GNFRAC} = \mathrm{FIFNGB} \tag{11.4-2}$$

The unit of FISGAS(I,J) in Eq. 11.4-1 is gm/cm^3. The default value of GBFRAC is 0.10.

The two other relevant input information required by FPIN2 are the plenum and cavity gas constants, PLGASR and GASCON, in Bar-cm^3/gm-K. For fresh fuel pins (BURNFU=0) these constants are simply calculated from

$$\mathrm{GASCON} = \mathrm{PLGASR} = \frac{\mathrm{RGASSI}}{\mathrm{HEMM}} 1\cdot 10^{1} \tag{11.4-3}$$

For irradiated pins (BURNFU≠0) the following formulas are used

$$\mathrm{GASCON} = \frac{\mathrm{RGASSI}}{\mathrm{FGMM}} 1\cdot 10^{1} \tag{11.4-4}$$

$$\mathrm{PLGASR} = \frac{\mathrm{RGASSI}\cdot \mathrm{POGAS}\cdot 1\cdot 10^{1}}{\mathrm{POGAS}\cdot \mathrm{FGMM} - (1-\mathrm{FGFI})\cdot 1.0133\cdot 10^{5}\cdot(\mathrm{FGMM}-\mathrm{HEMM})} \tag{11.4-5}$$

11.4.3.3 Porosity Distribution

The porosity distribution is also input into FPIN2 (through PORES(I,J) variable). As given in the input description in Table 11.4-3, these values are the total porosity of the nodes, exclusive of the volume of any macroscopic cracks (crack volumes are specified separately as input). The difference between the total porosity and the grain boundary bubble porosity is equal to the porosity of the large pores that are free of surface tension restraint. These large pores may be interconnected (open) or closed. In FPIN2, however, all large pores are assumed to be open and fission gas residing in the open porosity after steady-state irradiation is calculated from the local open pore volume and temperature assuming that the pore pressure is in equilibrium with the plenum pressure. This gas is assumed to be trapped in the fuel during transient heating.

Few measurements of porosity distributions are available for the metallic fuels. Therefore, the fractional porosity is generally determined from the fuel geometry, the fuel mass, and the fuel and fission product densities assuming a uniform distribution. In SASSYS/SAS4A, porosity distribution is specified on a zone-by-zone basis using the porosity values for eight fuel types (PRSTY in Block 13, locations 1073-1080) as described in section 11.4.3.1. Integrated model interfaces with an internal SASSYS/SAS4A array variable (PRSTY2(I,J) to get final distribution on a node-by-node basis.

The magnitude and distribution of the total porosity do not play a large role in mechanics calculation as long as there is sufficient volume to accommodate the grain boundary bubbles so that the resultant open porosity is greater than zero. The FPIN2 models assume that the open porosity does not contribute to solid fuel swelling or to hot pressing because.

1. Sodium logging may partially fill the pores,
2. Driving pressures for swelling are small since the voids are connected to the plenum,
3. Most of the voids are probably large enough so that the time constants for their growth are long compared to the span of the accident transient [11-14].

The distribution of open porosity does not significantly influence the mechanics results either. Although fission gas in the open pores is trapped at the time of fuel melting, its pressure is in equilibrium with the plenum pressure so that this gas contributes little to molten fuel expansion. Most of the expansion comes from the grain boundary gas or the gas in solution in the fuel matrix that has significant swelling potential when it collects into large bubbles following fuel melting. Coalescence of small bubbles into large bubbles is very rapid in liquid fuel [11-20] and is assumed to occur instantaneously in the FPIN2 calcualtion of molten fuel extrusion.

11.4.3.4 Cladding Fluence

The axial distribution of the cladding fluence is needed in life fraction correlation evaluations. In the integrated SAS-FPIN2 model, this variable is determined from the following formula

$$CLDFLU(J) = 8.64 \cdot 10^{-22} \frac{FPDAYS \cdot FLTPOW \cdot PBAR(J)}{AXHI(J)} \quad (11.4\text{-}6)$$

Were FPDAYS, FLTPOW, and AXHI(J) are SASSYS/SAS4A input variables, and PBAR(J) is an internal SASSYS/SAS4A array variable. The unit of CLDFLU(J) in this equation is 10^{22} neutrons/cm^2. For applications where fast-flux to linear-power ratio (FLTPOW in Block 62, location 61) is not available, cladding fluence is approximately set equal to the burnup in at.% (i.e., BURNFU in Block 65, location 54).[8]

11.4.3.5 Length of Sodium in Plenum

The initial length of sodium in the pin plenum is expected to be specified for hot and irradiated conditions in FPIN2. In the integrated model, this value is calculated internally using SASSYS/SAS4A subroutine NABOND. This subroutine evaluates the gap thickness for each axial segment and determines the amount sodium in the plenum from initial mass of sodium added to produce the fuel-cladding bound (BONDNA in Block 63, location 71). The length in sodium in the plenum then is calculated from plenum geometry consistent with the steady-state temperature distribution.

11.4.3.6 Effective Cladding Inner Surface Wastage

The integrated SAS-FPIN2 model provides an extended capability to include the effects of cladding wastage on fuel element mechanics that is not an original part of the FPIN2 code. The SAS-FPIN2 interface has been modified to include two SASSYS/SAS4A input variables describing initial wastage thicknesses on the cladding inner and outer surfaces (TWASTI and TWASTO in Block 61, locations 272 and 273, respectively.)

Cladding wastage is typically considered in design-basis safety assessments. The bases of the wastage in metallic fuel elements are the scratches on the cladding surfaces, diffusion of fuel constituents and fission products into the cladding, and the eutectic formation at the fuel cladding interface. Diffusion of fuel and fission products creates a lanthanide rich FCCI zone that has distinctly different microstructure with cracks and it is assumed to be strengthless. In addition, a separate carbon depleted band with decreased hardness is often identified next to the FCCI zone in HT9 cladding. Although this region exhibits only a moderate decrease in strength, it can conservatively be considered as part of the wastage for the safety cases.

In the integrated SAS-FPIN2 model, effective inner surface wastage is defined as the sum of inner and outer surface wastages and it is incorporated into the mechanics calculation by defining them as part of an FPIN2 variable describing the cladding eutectic penetration. This allows consideration of the wastage bands as part of the cladding for heat transfer while the stress field is determined considering only the thickness of unaffected cladding that is available to carry the load.

[8] EBR-II specific, may not be valid for other reactors.

11.4.4 Output Description and Graphics File Usage

A brief description of the output generated by FPIN2 in the interfaced mode is as follows. A sample of the regular output for fuel/cladding summary information and plenum/molten cavity results is shown in Fig. 11.4-4. In the first part of the output, FPIN2 mechanics results are printed for each axial segment separately. The descriptions of the variables printed in this category are presented in Table 11.4-4. FPIN2 regular output for each axial segment is followed by a summary of plenum/molten cavity results as shown in the bottom portion of Fig. 11.4-4. The description of the variables printed in this category is presented in Table 11.4-5.

In addition to regular FPIN2 output described above, a series of diagnostic messages are also printed as part of SASSYS/SAS4A output as the integrated model calculations progress. These diagnostic messages can be categorized as follows:

1. Messages regarding the execution of the FPIN2 such as non-convergent iterations and maximum iteration warnings in various parts of the program, and occurrence of non-positive definite matrix,
2. Messages regarding the non-physical phenomena such as negative gas pressure, inconsistent input for constitutive equation options, or negative open porosity,
3. Information messages regarding the cladding failure in a particular axial segment, fuel-cladding gap mixup, complete cladding melting, and cavity solidification stop.

A summary of these messages is also printed at the end of the transient calculations.

The FPIN2 detailed output option can be invoked by setting the input flag LOUTSW=1 (Block 51, location 296). This option generates a huge printout for the details of FPIN2 calculations and it is used for debugging purposes only. The information printed under this option is generally self-explanatory; therefore, it is not discussed separately here. The print frequency of the regular and detailed FPIN2 output discussed above is controlled by the same SASSYS/SAS4A input parameters that control DEFORM5 output.

For graphics use, some of the variables printed in regular output are stored in binary form in a graphics file at every time step by invoking the option LGRPAH=1 (Block 51, location 300). The logical unit number assigned for FPIN2 graphics file is 23. The list of variables printed in the graphics file is presented in Table 11.4-6.

SAS4A 3.0 SAS-FPIN2 INTEGRATED MODEL VALIDATION. T.SOFU, NOVEMBER 1993 11/ 5/93 14:45:15 PAGE 140 CHANNEL 1
JOB: 12734/glow TREAT M7 PIN 1 : 9.8% BURNUP U-19PU-10ZR FUEL in D9 CLAD USER: 45019/sofu

FPIN2 OUTPUT FOR METAL FUELED ELEMENTS

CHANNEL = 1
TIME STEP = 700
TIME = 17.500

NODE (J)	PCAV (PA)	VGCAV (CC)	RCAV (CM)	WFUEL (MM)	FCGAP (MM)	PFC (PA)	RCMELT (CM)	TCMID (K)	SIGAV (PA)	EPSPTMID	WCLAD (MM)	CLIFE	CLDPR (%)
20	0.201E+08	0.0451	0.2152	0.0406	0.0000	0.205E+08	0.0000	1220.0	0.134E+09	0.00213	0.0238	0.701	0.00
19	0.201E+08	0.0442	0.2149	0.0410	0.0000	0.208E+08	0.0000	1204.5	0.136E+09	0.00143	0.0233	0.487	0.00
18	0.201E+08	0.0435	0.2146	0.0412	0.0000	0.211E+08	0.0000	1187.2	0.137E+09	0.00094	0.0227	0.322	0.00
17	0.201E+08	0.0430	0.2144	0.0410	0.0000	0.216E+08	0.0000	1167.6	0.139E+09	0.00061	0.0219	0.200	0.00
16	0.201E+08	0.0316	0.1855	0.0419	0.0000	0.226E+08	0.0000	1145.5	0.145E+09	0.00038	0.0210	0.115	0.00
15	0.201E+08	0.0315	0.1853	0.0411	0.0000	0.231E+08	0.0000	1121.2	0.148E+09	0.00021	0.0200	0.061	0.00
14	0.201E+08	0.0315	0.1852	0.0399	0.0000	0.236E+08	0.0000	1094.8	0.151E+09	0.00011	0.0190	0.032	0.00
13	0.201E+08	0.0315	0.1850	0.0385	0.0000	0.240E+08	0.0000	1067.7	0.154E+09	0.00006	0.0179	0.017	0.00
12	0.201E+08	0.0221	0.1560	0.0379	0.0000	0.255E+08	0.0000	1039.8	0.164E+09	0.00003	0.0167	0.011	0.00
11	0.201E+08	0.0220	0.1559	0.0356	0.0000	0.261E+08	0.0000	1011.2	0.168E+09	0.00004	0.0156	0.008	0.00
10	0.201E+08	0.0217	0.1557	0.0327	0.0000	0.268E+08	0.0000	982.1	0.172E+09	0.00007	0.0145	0.006	0.00
9	0.201E+08	0.0213	0.1556	0.0302	0.0000	0.276E+08	0.0000	952.8	0.176E+09	0.00008	0.0134	0.004	0.00
8	0.201E+08	0.0208	0.1555	0.0271	0.0000	0.282E+08	0.0000	923.3	0.180E+09	0.00010	0.0122	0.002	0.00
7	0.201E+08	0.0119	0.1262	0.0116	0.0000	0.353E+08	0.0000	892.9	0.228E+09	0.00012	0.0116	0.001	0.00
6	0.201E+08	0.0066	0.0976	0.0106	0.0000	0.420E+08	0.0000	862.1	0.273E+09	0.00014	0.0106	0.001	0.00
5	0.201E+08	0.0000	0.0000	0.0096	0.0000	0.611E+08	0.0000	830.1	0.402E+09	0.00014	0.0096	0.000	0.00
4	0.201E+08	0.0000	0.0000	0.0084	0.0000	0.620E+08	0.0000	798.2	0.408E+09	0.00011	0.0084	0.000	0.00
3	0.201E+08	0.0000	0.0000	0.0072	0.0000	0.625E+08	0.0000	767.0	0.411E+09	0.00007	0.0072	0.000	0.00
2	0.201E+08	0.0000	0.0000	0.0061	0.0000	0.638E+08	0.0000	736.2	0.420E+09	0.00004	0.0061	0.000	0.00
1	0.201E+08	0.0000	0.0000	0.0050	0.0000	0.625E+08	0.0000	706.3	0.412E+09	0.00000	0.0050	0.000	0.00

FPIN2 MOLTEN CAVITY/PLENUM RESULTS

CVGAST (K)	VOLCV (CC)	VFSOL (CC)	VFLIQ (CC)	CVGASV (CC)	PPLEN (PA)	PLGAST (K)	PLGASV (CC)	PLNAV (CC)	EXTRUS (CC)	WFTOT (CM)	WCTOT (CM)	F-TAVE (K)	C-TAVE (K)
1480.56	2.68941	0.98909	1.27209	0.65765	0.201E+08	1124.34	3.55729	1.78952	0.22942	0.5398	0.2976	1295.5	985.5

Fig. 11.4-4: FPIN2 Regular Output for Fuel Element Mechanics Summary

Table 11.4-4: Description of the variables in FPIN2 Regular Output for Fuel Element Mechanics Summary

Variable	Unit	Description
PCAV	(Pa)	Molten fuel cavity pressure
VGCAV	(cm^3)	Volume of gas in molten fuel cavity
RCAV	(cm)	Outer radius of the molten fuel cavity
WFUEL	(mm)	Axial displacement of fuel column segment
FCGAP	(mm)	Fuel-cladding gap thickness
PFC	(Pa)	Contact pressure between the fuel and cladding (plenum pressure if gap is open)
RCMELT	(cm)	Radius of cladding melting
TCMID	(K)	Temperature of cladding at radial midpoint
SIGAV	(Pa)	Average hoop stress in cladding
EPSPTMID		Plastic hoop strain in cladding at radial midpoint
WCLAD	(mm)	Axial displacement of cladding segment
CLIFE		Cladding life fraction
CLDPR	(%)	Eutectic penetration of the cladding

Table 11.4-5: Description of the Variable in FPIN2 Regular Output for Plenum/Multen Cavity Results

Variable	Unit	Description
CVGAST	(K)	Molten fuel average temperature
VOLCV	(cm^3)	Total molten cavity volume
VFSOL	(cm^3)	Volume of fuel in molten cavity between solidus and liquidus
VFLIQ	(cm^3)	Volume of fuel in molten cavity above liquidus
CVGASV	(cm^3)	Volume of fuel vapor in molten cavity
PPLEN	(Pa)	Pin plenum pressure
PLGAST	(K)	Pin plenum average temperature
PLGASV	(cm^3)	Volume in pin plenum available to gas
PLNAV	(cm^3)	Volume of sodium in plenum
EXTRUS	(cm^3)	Volume of molten fuel extruded into the plenum
WFTOT	(cm)	Total axial displacement of fuel
WCTOT	(cm)	Total axial displacement of cladding
F-TAVE	(K)	Average temperature of entire fuel column
C-TAVE	(K)	Average temperature of cladding tube containing fuel

Table 11.4-6: Description of the Variables Stored in FPIN2 Binary Graphics File (Logical Unit #23)

Order	Variable	Unit	Description
1	TIME	(s)	Current time at which values of the variables are reported
2	PCAVTY	(Pa)	Molten fuel cavity pressure
3	CVGAST	(K)	Molten fuel cavity temperature
4	AMELTF(NDZ)	(%)	Areal (radial) melt fraction for the top axial segment
5	PPLEN	(Pa)	Pin plenum pressure
6	PLGAST	(K)	Pin plenum temperature
7	PFC(NDZ)	(Pa)	Fuel-cladding contact pressure at top axial segment
8	SIGCM(NDZ)	(Pa)	Cladding average hoop stress in top axial segment
9	EPSPTM(NDZ)		Cladding average plastic hoop strain in top axial segment
10	FRCPEN(NDZ)	(%)	Cladding eutectic penetration at top axial segment
11	XLIFEF(NDZ)		Cladding life fraction for top axial segment
12	WCTOT	(cm)	Total cladding axial displacement
13	WFTOT	(cm)	Total fuel axial displacement
14	EXTRUL	(cm)	Length of molten fuel extruded into plenum
15	FUELTL	(cm)	Total fuel elongation
16	TCLADM(NDZ)	(K)	Average cladding temperature in top axial segment

REFERENCES

11-1. T. H. Hughes, Unpublished information, Argonne National Laboratory, 1977.

11-2. M. Rossow, T. H. Hughes, and J. M. Kramer, Unpublished information, Argonne National Laboratory, 1981.

11-3. T. H. Hughes, Unpublished information, Argonne National Laboratory, 1985.

11-4. T. H. Hughes and J. M. Kramer, "The FPIN2 Code – An Application of the Finite Element Method to the Analysis of the Transient Response of Oxide & Metal Fuel Elements," *Proc. Conf. Sci. & Tech. Fast Reactor Safety*, Guersney, May 1986.

11-5. J. M. Kramer, T. H. Hughes, and E. E. Gruber, Unpublished information, Argonne National Laboratory, 1987.

11-6. J. M. Kramer, T. H. Hughes, and E. E. Gruber, "Validation of Models for the Analysis of the Transient Behavior of Metallic Fast Reactor Fuel," *Proc. Int. Conf. Structural Mechanics in Reactor Technology*, Anaheim, California, vol C, pp. 65-76, August 1989.

11-7. G. L. Hofman, et al., Unpublished information, Argonne National Laboratory, 1985.

11-8. H. L. Schreyer, Unpublished information, Argonne National Laboratory, 1980.

11-9. J. M. Kramer, Unpublished information, Argonne National Laboratory, 1977.

11-10. J. M. Kramer and T. H. Hughes, "Modeling of Fuel Cracking and Fuel Plasticity in LMFBR Fuel Pins During Accident Transients," *Proc. Seminar in Mathematical/Mechanical Modeling of Reactor Fuel Elements*, August 1977.

11-11. A. C. Eringen, Nonlinear Theory of Continuous Media, McGraw-Hill, New York, 1962.

11-12. J. M. Kramer and T. H. Hughes, Unpublished information, Argonne National Laboratory, 1993.

11-13. R. G. Pahl, et al., Unpublished information, Argonne National Laboratory, 1986.

11-14. E. E. Gruber and J. M. Kramer, Unpublished information, Argonne National Laboratory, 1985.

11-15. T. H. Bauer, G. R. Fenske, and J. M. Kramer, "Cladding Failure Margins for Metallic Fuel in the Integral Fast Reactor," *Proc. 9th Int. Conf. Structural Mechanics in Reactor Technology*, Lausanne, vol. C, pp. 31-38, 1987.

11-16. W. F. Brizes and M. L. Hamilton, Unpublished information, Hanford Engineering Development Laboratory, 1982.

11-17. F. R. Shober, Unpublished information, Hanford Engineering Development Laboratory, 1986.

11-18. M. C. Billone, Personal Communication (LIFE-METAL seminar Series), May 11, 1993.

11-19. W. F. Murphy, et al., “Post-irradiation Examination of U-Pu-Zr Fuel Elements Irradiated in EBR-II to 4.5 Atomic Percent Burnup,” ANL-7602, Argonne National Laboratory, November 1969.

11-20. J. M. Kramer, Unpublished information, Argonne National Laboratory, 1978.

APPENDIX 11.1
EXPLICIT FORMULAS FOR STIFFNESS MATRIX AND LOAD VECTOR

The stiffness matrix is defined in Section 11.2.4.2, Eq. 11.2-78.

$$[K] = \int_{A_c} [B]^T [C][B] dA \tag{A11.1-1}$$

where the form of [B] and [C] matrices depends on the type of fuel element considered. Introducing new variables

$$d = \frac{b}{r} - 1 \tag{A11.1-2}$$

$$e = 1 - \frac{a}{r} \tag{A11.1-3}$$

the matrix [B] can be written in a compact form as

$$[B] = \frac{1}{l}\begin{bmatrix} -1 & 1 & 0 \\ d & e & 0 \\ 0 & 0 & 1 \end{bmatrix} \tag{A11.1-4}$$

where *a*, *b*, and *l* are explained in Fig. 11.2-2. As noted in Section 11.2.4.1, this form of matrix [B] is valid for both continuous and cracked elements.

Expanding the matrix triple product in Eq. A11.101 and using the symmetry of [C] yields

$$[K] = \frac{1}{l^2}\int_{A_c} \begin{bmatrix} \left(C_{11} - 2C_{12}d + C_{22}d^2\right) & \left(-C_{11} + C_{12}\left(d-e\right) + C_{22}ed\right) & \left(-C_{13} + C_{23}d\right)l \\ \left(-C_{11} + C_{12}\left(d-e\right) + C_{22}ed\right) & \left(C_{11} - 2C_{12}e + C_{22}e^2\right) & \left(-C_{13} + C_{23}e\right)l \\ \left(-C_{13} + C_{23}d\right)l & \left(C_{13} + C_{23}e\right)l & C_{33}l^2 \end{bmatrix} dA \tag{A11.1-5}$$

Inspection of this equation indicates that all elements of [*K*] can be expressed in terms of following six integrals

$$I \equiv \int_{A_c} dA = \pi l\left(a+b\right) \tag{A11.1-6}$$

$$I_d \equiv \int_{A_c} \left(d\right) dA = \pi l^2 \tag{A11.1-7}$$

$$I_{d2} \equiv \int_{A_c} \left(d^2\right) dA = \pi l\left[\frac{2b^2}{l}\ln\left(\frac{b}{a}\right) - 3b + a\right] \tag{A11.1-8}$$

$$I_e \equiv \int_{A_c} \left(e\right) dA = \pi l^2 \tag{A11.1-9}$$

$$I_{e2} \equiv \int_{A_c} \left(e^2\right) dA = \pi l\left[b - 3a + \frac{2a^2}{l}\ln\left(\frac{b}{a}\right)\right] \tag{A11.1-10}$$

$$I_{ed} \equiv \int_{A_c} \left(ed\right) dA = \pi l\left[a + b - \frac{2ab}{l}\ln\left(\frac{b}{a}\right)\right] \tag{A11.1-11}$$

The domain of these integrations is shown in Fig. 11.2-2. In terms these newly defined variables, the stiffness matrix can be rewritten as

$$\left[K\right] = \frac{1}{l^2}\begin{bmatrix} \left(C_{11}I - 2C_{12}I_d + C_{22}I_{d2}\right) & \left(-C_{11}I + C_{12}\left(I_d - I_e\right) + C_{22}I_{ed}\right) & \left(-C_{13}I + C_{23}Id\right)l \\ \left(-C_{11}I + C_{12}\left(I_d - I_e\right) + C_{22}I_{ed}\right) & \left(C_{11}I - 2C_{12}I_e + C_{22}\,I_{e2}\right) & \left(C_{13}I + C_{23}I_e\right)l \\ \left(-C_{13}I + C_{23}I_d\right)l & \left(C_{13}I + C_{23}I_e\right)l & C_{33}Il^2 \end{bmatrix} \tag{A11.1-12}$$

The load vector for a pressure load acting in the radial direction in given by Eq. 11.2-67

$$t_i = \int_C \sigma_r N_i \hat{i}_r \cdot \hat{n}\, dC \tag{A11.1-13}$$

(i=1,2). The shape functions N_1 and N_2 are defined in Eqs. 11.2-63 and 11.2-64, respectively. For the case of an element bordering the central cavity, the curve C corresponds to the inner radius of the element, we have

$$\sigma_r = -p_{cav} \tag{A11.1-14}$$

$$\hat{i}_r \cdot \hat{n} = \hat{i}_r \cdot \left(-\hat{i}_r\right) = -1 \tag{A11.1-15}$$

$$N_1 = 1 \tag{A11.1-16}$$

$$N_2 = 0 \tag{A11.1-17}$$

$$\int_C dC = 2\pi r_{cav} \tag{A11.1-18}$$

Hence,

$$t_1 = 2\pi p_{cav} r_{cav} \tag{A11.1-19}$$

$$t_2 = 0 \tag{A11.1-20}$$

A similar derivation for an element experiencing a pressure p_{out} directed radially inward shows that

$$t_1 = 0 \tag{A11.1-21}$$

$$t_2 = 2\pi p_{cav} r_{out} \tag{A11.1-22}$$

where r_{out} is the outer radius of the element.

APPENDIX 11.2
LIST OF INPUT VARIABLES FOR STANDALONE FPIN2 CALCULATION

*** Location Numbers for Integer Data ***

(Number in parentheses following value name states maximum value)

***** COMMON/INPUTI/ *****

Location Number	Name	Value	Description
1	IFTYPE	=1	Uranium - 5% fissium fuel
		=2	Uranium - 10% zirconium fuel
		=3	Uranium - 15% plutonium - 10% zirconium fuel
		=4	User supplied mixture of U-Pu-Zr fuel (input required at loc. numb. 5001+ & 5401+)
2			(Not currently used)
3	ICTYPE	=1	20% CW type 316 cladding
		=2	D9 cladding
		=3	HT9 cladding
4			(Not currently used)
5	IDTOPT	=0	Compute at equally spaced time values (use NDT and DTIME)
		=1	Increments in time are user-supplied (use NDT and TTABLE)
6	IHTOPT	=0	Perform heat transfer calculation including coolant and wall
		=1	Perform heat transfer calculation with input values of clad outer surface temperature. (Use NCLADT and COMMON/TEMPIN)
7-14		(8)	(Not currently used)
15	ICRACK	=0	No fuel cracking
		=1	Radial fuel cracks included
16	IFPLAS	=0	Allow creep-plastic strains in fuel
		=1	Suppress creep-plastic strains in fuel
17	ICPLAS	=0	Allow creep-plastic strains in clad
		=1	Suppress creep-plastic strain in clad
18	IFSWEL	=0	Allow swelling-hotpressing strains in fuel
		=1	Suppress swelling-hotpressing strains in fuel

***** COMMON/INPUTI/ *****

Location Number	Name	Value	Description
19	ICSWEL	=0	Allow swelling strains in clad
		=1	Suppress swelling strains in clad
20	IDZ	=0	Axial segments are of equal height DZ=Z/NDZ
		=1	User-supplied axial segment heights
21	ILRGST	=0	Large strain analysis
		=1	Small perturbation analysis
22	IFCSLP	=0	Fuel-clad locked when gap is closed
		=1	Independent fuel-clad axial displacement
23			(Not currently used)
24	IOUTSW	=0	No detailed printing of results – summary of results only
		=1	Normal detailed printout under IFREQA, NFREQA, and IFREQB control
25	IFREQA		Initial print frequency, number of time steps between normal detailed printout
26	NFREQA		Total number of time steps under IFREQA control
27	IFREQB		Final print frequency
28	IGRAPH	=0	Do not write graphics file
		=1	Write datafile FT12F001 for processing by a graphics program
29-30		(2)	(Not currently used)
31	NDT		No. of time steps or no. of entries in TTABLE. If IDTOPT=0, there is no limitation on NDT. If IDTOPT=1, NDT is limited to 1980.
32	NDZ	(20)	No. of axial segments
33	NDRF	(20)	No. of radial elements in cladding (minimum value is 6)
34	NDRC	(10)	No. of radial elements in cladding (minimum value is 3)
35-40		(6)	(Not currently used)
41	NQ	(25)	No. of values in power vs. time table
42	NCOOLT	(25)	No. of values in coolant inlet temperature versus time table

*** COMMON/INPUTI/ ***			
Location Number	**Name**	**Value**	**Description**
43	NCOOLF	(25)	No. of values in coolant inlet flow versus time table
44	NCLADT	(50)	No. of values in clad outer surface temperature versus time table
45-100		(56)	(Not currently used)
101-500	IETYPI(I,J)	(20,20)	Fuel element type. Required only when ICRACK=1, default element type is 1 (Loc. Numb. = 100+I+20*(J-1)).

*** Location Numbers for Decimal Data ***

(Symbols in parentheses after array variables are maximum storage allocation and name of integer variable specifying dimension. Numbers within quotation marks are recommended values)

***** COMMON/CNTLIN/ *****

Location Number	Name	Value	Description
1	TZERO		Initial time (sec)
2	DTIME	=1	Computation time step (if IDTOPT=0) (sec)
3-10		(8)	(Not currently used)
11-2000	TTABLE	(1990 NDT)	Computation time steps (if IDTOPT=1) (sec) maximum of 1990 values

***** COMMON/GEOMIN/ *****

Location Number	Name	Value	Description
2001	ZFUEL		Length of fuel column (cm)
2002-2010		(9)	(Not currently used)
2011-2030	DZ	(20 NDZ)	Height of axial segments (cm) (required only when IDZ=1)
2031-2050	FUELIR	(20 NDZ)	Inner radius of fuel (cm)
2051-2070	FUELOR	(20 NDZ)	Outer radius of fuel (cm)
2071-2090	CLADIR	(20 NDZ)	Inner radius of clad (cm)
2091-2110	CLADOR	(20 NDZ)	Outer radius of clad (cm)
(Note: values #2111-2112 not required when IHTOPT=1)			
2111	WALLIR		Inner radius of outer wall (cm)
2112	WALLOR		Outer radius of outer wall (cm)
2113	ZPLENM		Total length of plenum (cm)
2114	ZPLNA		Length of sodium in plenum (cm)
2115	PLGASR		Gas constant for plenum gasses (Bar-cc/gm-K)

***** COMMON/GEOMIN/ *****

Location Number	Name	Value	Description
2116	PLTREF		Temperature at which PINT specified (K). Used to correct PINT to value consistent with initial plenum temperature.
2117-2200		(84)	(Not currently used)
2201-2600	FECTI(I,J)	(20,20 NDZ)	Initial radial crack strain in fuel (required only when ICRACK=1) (Loc. Numb.=2200+I+20*(J-1))
2601-3000		(400)	(Not currently used)

***** COMMON /DRIVIN/ *****

Location Number	Name	Value	Description
3001	PEXT		External pressure. Assumed constant during transient. (Bar)
3002	PINT		Initial value of internal pin press. (Bar)
3003-3004		(2)	(Not currently used)
(Note: values 3005-3006 not needed when IHTOPT=1)			
3005	TSINK		Temperature of outer heat sink (K)
3006	HSINK		Heat transfer coefficient-wall to outer heat sink (Watts/cm^2-K)
3007	QCONST		Energy generation constant. The energy generation rate for fuel radial segment I, axial segment J at time K is calculated as: QCONST*QR(I)*QAX(J)*QT(K) The method of dimensioning and normalizing the four factors is arbitrary so long as the product dimension is in Watts/gm.
3008	BURNUP		Peak fuel burnup (atom %)
3009-3010		(2)	(Not currently used)

***** COMMON /DRIVIN/ *****

Location Number	Name	Value	Description
3011-3410	QR(I,J)	(20,20 NDZ)	Radial profile of energy generation rate. Values are required for NDRF radial elements in each axial segment. (See: QCONST for units) (Loc. Numb. = 3010+I+20*(J-1))
3411-3430	QAX	(20 NDZ)	Axial profile of energy generation rate (see: QCONST)
3431-3455	TQT	(25 NQ)	Time values in power vs. time table (sec)
3456-3480	QT	(25 NQ)	Power values in power vs. time table (see: QCONST)
(Note: values 3481-3580 not needed when IHTOPT=1)			
3481-3505	TTIN	(25 NCOOLT)	Time values in coolant inlet temperature versus time table (sec)
3506-3530	TIN	(25 NCOOLT)	Coolant inlet temperatures (K)
3531-3555	TCFIN	(25 NCOOLF)	Time values in coolant inlet flow versus time table (sec)
3556-3580	CFIN	(25 NCOOLF)	Coolant inlet flow (gm/cm^2-sec)
3581-4000		(420)	(Not currently used)

***** COMMON /MISCIN/ *****

Location Number	Name	Value	Description
4001	GBFRAC		Fraction of FISGAS on grain boundaries (default value is 0.1)
4002-4039		(38)	(Not currently used)
4040	GASCON		Gas constant for central cavity gases (Bars-cc/gm-K)
4041-4060	CLDFLU	(20 NDZ)	Axial profile of clad fluence used in subroutine CFAIL (10^{22} n/cm^2)

***** COMMON /MISCIN/ *****

Location Number	Name	Value	Description
4061-4080	CLDHRD	(20 NDZ)	Pre-transient hardness parameter used in clad flow stress calculation. (Default value is 0.223, the value appropriate to 20% CW unirradiated stainless steel.)
4081-4480	PORES(I,J)	(20,20 NDZ)	Dist. of total fuel porosity same radial grid as QR (do not include crack volume input) (Loc. Numb. = 4080+I+20*(J-1))
4481-4880	FISGAS(I,J)	(20,20 NDZ)	Dist. of fission gas (gm/cc) in fuel closed porosity and in solution on same radial grid as QR (do not include fission gas in open porosity). (Loc. Numb. = 4480+I+20*(J-1))
4881-5000		(120)	(Not currently used)
5001-5400	FRACPU(I,J)	(20,20 NDZ)	Dist. of plutonium (wt. %) in fuel (required when IFTYPE=4) (Loc. Numb. = 5000+I+20*(J-1))
5401-5800	FRACZR(I,J)	(20,20 NDZ)	Dist. of zirconium (wt. %) in fuel (required when IFTYPE=4) (Loc. Numb. = 5400+I+20*(J-1))
5801-6000		(200)	(Not currently used).

***** COMMON TEMPIN/ *****

Location Number	Name	Value	Description
(Note: values 6001-7050 are only required when IHTOPT=1)			
6001-6050	TVALUE	(50 NCLADT)	Time values for clad surface temperature table (include TZERO) (sec)
6051-7050	TCSURF(J,K)	(20 NDZ, 50 NCLADT)	Clad outer surface temperature for axial segment J at time K (K) (Loc. Numb. = 6050+J+20*(K-1))

*** Location Numbers for Debug Data ***

(All debug options default to zero. Therefore, input is required only if a debug option is to be used. Debug input is identified with location numbers larger than 9000 and it follows same conventions as regular input. Integer debug data is read in with regular integer data and decimal debug data is read in with regular decimal data.)

***** COMMON /DEBUGI/ --- Integer Debug Data *****

Location Number	Name	Value	Description
9001	IDBOUT	=0	No debug output
		=1	Add debug output to regular IOUTSW=2 output
9002	IDBSTP	=0	Program stops when molten cavity freezes
		=1	Ignore this program stop
9003	IDBFPL	=0	Use recommended fuel flow stress (Eq. 11.3-16)
		=1	Use simple power law fuel creep: $\dot{\varepsilon} = C_0 * \sigma_e^{C_1}$ (Decimal values 9001 and 9002 are required)
9004	IDBFDV	=0	Use recommended fuel swelling – hotpressing (fuel swelling option for metal fuel is the simple grain boundary swelling model (ANL-IFR-27) & (ANL/RAS 83-33)
		=1	Use equilibrium swelling model (ANL-IFR-6 and -23)
		=2	Use simple power law fuel swelling: $\dot{\varepsilon} = C_0 * \sigma_m^{C_1}$ (Decimal values 9003 & 9004 are required)
9005	IDBCPL	=0	Use recommended clad flow stress
		=1	Use ideal plastic flow for clad: $\sigma_y = C_0 + C_1 \bar{\varepsilon}^p$ (Decimal values 9005 & 9006 are required)
		=2	Use high-temperature power-law creep
		=3	Use simple power law clad creep: $\dot{\varepsilon} = C_0 * \sigma_e^{C_1}$ (Decimal values 9005 & 9006 are required)

***** COMMON /DEBUGI/ --- Integer Debug Data *****

Location Number	Name	Value	Description
9006	IGPRES	=0	Open fuel-clad gap pressure and plenum pressure remain at input values
		=1	User supplied gap pressure. This option allows FPIN2 to calculate pressure transients in gas pressurized cladding tubes. Plenum pressure is set equal to p_{gap}.
9007	IGAPCL	=0	Use fuel-clad opening/closure model
		=1	Fuel-clad gap always closed
9008	ICPROP	=0	Use material property correlations
		=1	Use temperature independent material properties
9009	ISKIPM	=0	Perform complete thermal/mechanical calculations
		=1	Bypass mechanical calculation, heat trans. only
9010	IGCLOS	=0	Use gap closure routine at 100% fuel melting
		=1	Do not close gap (if open) at 100% fuel melting
9011-9050		(40)	(Not currently used)
9051	NGPRES	(25)	No. of values in p_{gap} vs. time table
9052-9100		(49)	(Not currently used)
9101-9120	IDBOTA	(20 NDZ)	Axial debug print vector (0=no prt, 1=prt)
9121-9140	IDBOTF	(20)	Fuel radial debug print vector
9141-9150	IDBOTC	(10)	Clad radial debug print vector

***** COMMON /DEBUGD/ --- Decimal Debug Data *****

Location Number	Name	Value	Description
9001	FPLC0		Fuel power law creep constant C_0
9002	FPLC1		Fuel power law creep constant C_1
9003	FDVC0		Fuel power law swelling constant C_0
9004	FDVC1		Fuel power law swelling constant C_1
9005	CIPLC0		Clad idealized flow stress constant C_0

*** COMMON /DEBUGD/ --- Decimal Debug Data ***			
Location Number	**Name**	**Value**	**Description**
9006	CIPLC1		Clad idealized flow stress constant C_1
9007	HTERR		Relative convergence criterion for heat transfer calculation (ND) “0.0005”
9008	EPSCAV		Rel. convergence criterion for cavity pressure (ND) “0.001”
9009	EPSFE		Rel. convergence criterion for finite element analysis (ND) “0.0005”
9010	EPTEST		Rel. convergence criterion for plastic-creep strains (ND) “0.0005”
9011	EVTEST		Rel. convergence criterion for swelling strains (ND) “0.0005”
9012-9020		(9)	(Not currently used)
9021-9045	TGPRES	(25 NG PRES)	Time values in p_{gap} table
9046-9070	GPRES	(25 NGPRES)	Fuel-cladding gap pressure in p_{gap} table